Lithos 113 (2009) 158–178

Contents lists available at ScienceDirect

Lithos

journal homepage: www.elsevier.com/locate/lithos

Geochemistry and tectonic evolution of the Neoproterozoic Wadi Ghadir ophiolite, Eastern Desert, Egypt

Yasser Abd El-Rahman [a,b,*], Ali Polat [a], Yildirim Dilek [c], Brian Fryer [a,d], Mohamed El-Sharkawy [b], Shawki Sakran [b]

[a] Department of Earth and Environmental Sciences, University of Windsor, Windsor, ON, Canada N9B 3P4
[b] Geology Department, Cairo University, Giza, 12613 Egypt
[c] Department of Geology, Miami University, Oxford, OH, 45056 USA
[d] Great Lake Institute for Environmental Research, University of Windsor, ON, Canada N9B 3P4

ARTICLE INFO

Article history:
Received 17 July 2008
Accepted 24 December 2008
Available online 4 February 2009

Keywords:
Ophiolites
Ophiolitic mélange
Back-arc basin
Active continental margin
Arabian–Nubian Shield
Egypt

ABSTRACT

We report new geochemical data from the Neoproterozoic ophiolite in the Wadi Ghadir area, Eastern Desert, Egypt. The Wadi Ghadir ophiolite (WGO) is composed of layered and isotropic gabbros and amygdaloidal to porphyritic pillow lavas. Both the gabbroic rocks and the pillow lavas are intruded by dike swarms with different chemical affinities and spatial orientations. The WGO occurs in an ophiolitic mélange (Wadi Ghadir mélange, WGM), and both the WGO and WGM are intruded by granitic rocks to the west.

On the basis of Zr and Y variations, units of the WGO are classified as tholeiites (e.g., gabbros, amygdaloidal pillow lavas, D1, and D3 dikes). The late-stage D4 dikes show a calc-alkaline affinity, whereas porphyritic pillow lavas and D2 dikes have a transitional character. All ophiolitic units display subduction zone trace element signatures characterized by the enrichment of LILE over HFSE and negative Nb–Ta anomalies. Tholeiitic rocks are further divided into LREE-depleted (gabbros, D3 dikes) and LREE-enriched (amygdaloidal pillow lavas, D1 dikes) groups. Light REE-depleted tholeiitic rocks were derived from melting of a slightly depleted mantle source, whereas the LREE-enriched tholeiitic rocks were derived from a fertile N-MORB source. Calc-alkaline D4 dikes are characterized by steep REE patterns and have low Zr/Nb ratios (23–29), indicating melt contribution from an enriched mantle source, such as sub-continental lithospheric mantle and/or garnet peridotite. The transitional group has LREE-enriched patterns, but its degree of REE enrichment and Zr/Nb ratios are intermediate between the tholeiitic and calc-alkaline groups.

The WGO is interpreted to have formed in a back-arc setting behind the Nugrus volcanic arc developed above a NE-dipping subduction zone. The collision of this arc–back-arc system with the passive margin of the Nubian shield (Hafafit dome) resulted in the accretion of the Nugrus arc and the WGO onto the Nubian continental margin and in the initiation of a new subduction zone dipping SW beneath the newly accreted arc–back-arc crust and Hafafit dome. The establishment of this new Andean-type continental margin produced the calc-alkaline D4 dikes, leucogabbros and granitoid plutons intrude the Hafafit dome, the WGO, and the ophiolitic mélange.

1. Introduction

Preservation of ophiolitic rocks in the geological record has important implications for understanding the evolution of ancient orogenic belts (Dilek, 2003). Given that ophiolites are fragments of ancient oceanic lithosphere that were tectonically accreted to continental margins, they provide evidence for seafloor spreading and closure of ocean basins along convergent plate margins (Stern, 2004). The Neoproterozoic Era is unique in Earth history because it marks the widespread formation of ophiolites (Stern, 2005). Neoproterozoic ophiolites are especially common in the Arabian–Nubian Shield (ANS) and in the Central Asian Orogenic Belt (CAOB) (Şengör and Natal'in, 2004; Stern, 2005, 2007). Ages of the ANS ophiolites are tightly clustered around 870 to 690 Ma (Dilek and Ahmed, 2003; Stern et al., 2004), in comparison to ages of CAOB ophiolites which range from ~1000 Ma to Permian (Kröner et al., 2007).

The Eastern Desert of Egypt is part of the Neoproterozoic ANS. The ANS is separated by the Red Sea into Nubian Shield in northeast Africa and the Arabian Shield in western Arabia. The ANS represents the northern part of the East African Orogen (EAO), a large orogenic system formed near the end of the Proterozoic by collision between East and West Gondwana during the Pan-African orogeny (Stern, 1994).

Deciphering the tectonic settings of the ophiolites in the ANS is an important step for understanding the evolution of the Pan-African orogeny. The tectonic setting and evolution of Proterozoic ophiolites in the ANS remain controversial (Zimmer et al., 1995; Şengör and Natal'in, 1996; El Sayed et al., 1999; Reischmann, 2000; Dilek and Ahmed, 2003;

* Corresponding author. Department of Earth and Environmental Sciences, University of Windsor, Windsor, ON, Canada N9B 3P4.
E-mail address: yasser@uwindsor.ca (Y.A. El-Rahman).

0024-4937/$ – see front matter © 2009 Elsevier B.V. All rights reserved.
doi:10.1016/j.lithos.2008.12.014

Farahat et al., 2004; Stern et al., 2004). Ophiolites of the central Eastern Desert (CED) of Egypt occur as dismembered blocks in a tectonic mélange (Shackleton et al., 1980; Ries et al., 1983; Church, 1988; El Gaby et al., 1988). According to Sultan et al. (1992) and Abdelsalam and Stern (1996), the ophiolitic mélange in the CED is a result of deformation by the post-accretionary Najd fault system and therefore does not represent a suture zone. El Sharkawy and El Bayoumi (1979) and El Bayoumi (1980) were pioneers in identifying the Neoproterozoic oceanic crust in the Wadi Ghadir. On the basis of the geochemistry of the ophiolitic rocks, El Bayoumi (1980) proposed a similarity to MORB affected by plume-related magma. Kröner (1985) suggested a marginal basin tectonic setting for the origin of these Neoproterozoic oceanic rocks. Using the geochemistry of the pillow lavas, Farahat et al. (2004) proposed an ensialic back-arc basin setting for ophiolitic rocks in the CED, including the WGO.

The ANS ophiolitic mantle is composed mainly of tectonized harzburgite with lherzolite and is extensively serpentinized (Stern et al., 2004). On the basis of spinel compositions, two different tectonic settings have been inferred for the peridotites in the Eastern Desert ophiolites. Ahmed et al. (2001) proposed that the ophiolitic harzburgite is either a fragment of oceanic lithosphere modified by arc-related magmas or a fragment of back-arc basin lithosphere. Azer and Stern (2007) suggested that the serpentinized peridotites of the Eastern Desert ophiolites resemble peridotites from modern oceanic forearcs. The serpentinites of the WGO are interpreted to be derived from harzburgite–dunite parental rocks formed at a mid-ocean ridge and subsequently emplaced in a subduction zone setting (Khalil, 2007). The petrogenesis and mantle source composition of the crustal rocks of the WGO are therefore poorly understood.

We present new geochemical data for forty six samples from the WGO units (gabbros, pillow lavas and cutting dikes) and twenty two samples from the surrounding ophiolitic mélange. The objectives of this study are: (1) to document the geochemistry and petrogenesis of the WGO and cross-cutting dikes; (2) to evaluate the composition of the mantle source of the ophiolitic magmas; and (3) to present a geodynamic model for the evolution of the WGO.

2. Geology of the WGO

The Wadi Ghadir area is located in the central part of the Eastern Desert of Egypt and is occupied by a Neoproterozoic ophiolitic mélange composed mainly of ophiolitic fragments embedded in a sheared serpentinite and pelitic matrix (Fig. 1a,b). The ophiolitic rocks were described in detailed by El Bayoumi (1980). He reported the best exposure of ophiolitic rocks which occurs along Wadi El Beda and Wadi Saudi, the southwestern and western extensions of Wadi Dob Nia, which is a tributary of Wadi Ghadir (Fig. 1b). The ophiolite in Wadi

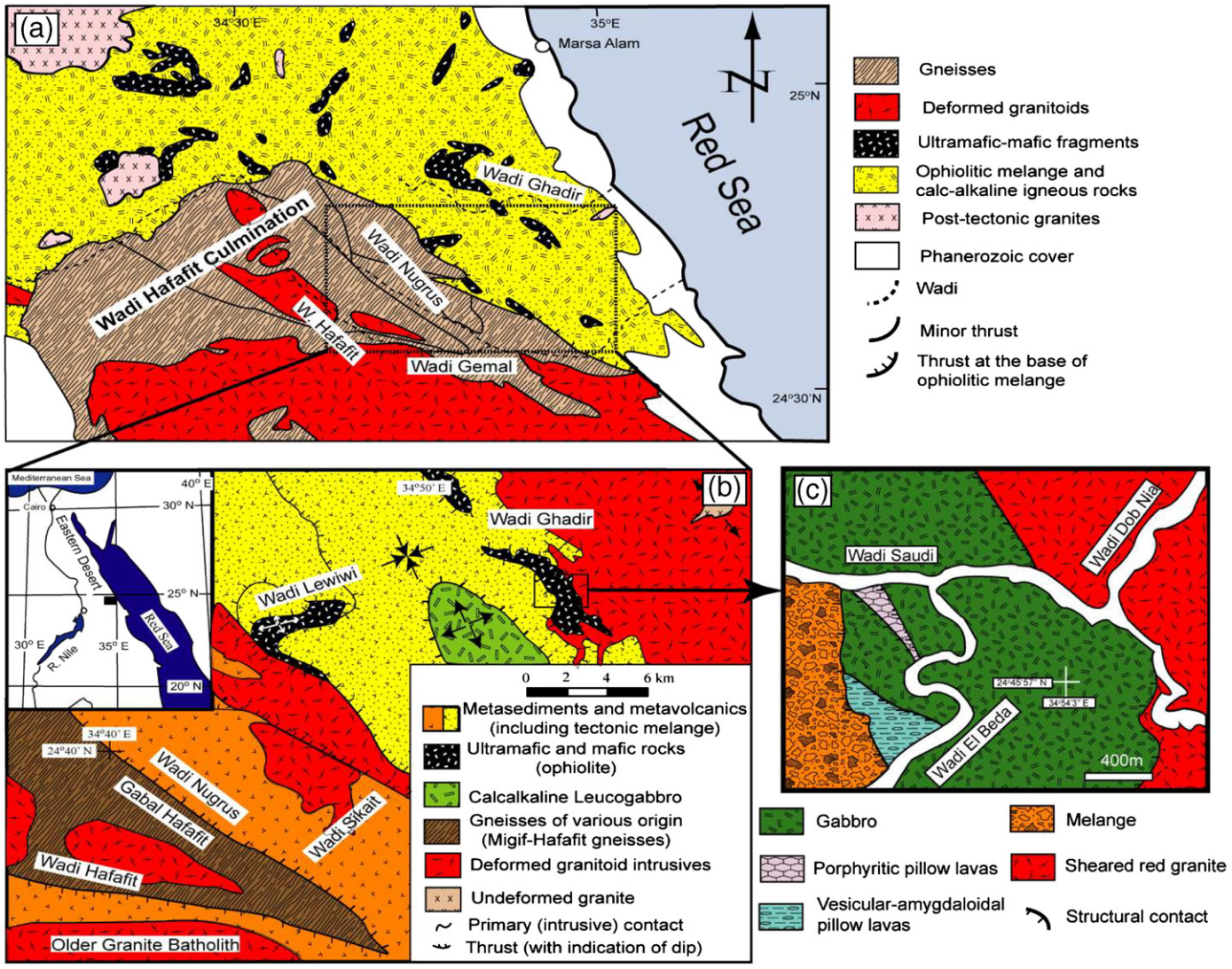

Fig. 1. (a) Schematic map showing major rock types exposed to the west of Marsa Alam (Kröner et al., 1987). (b) Simplified geological map for the area extending from Wadi Ghadir in the northeast to Hafafit area in the southwest. Converging and diverging arrows define interference structure of basin and dome respectively. (El Bayoumi and Greiling, 1984). (b) Geological map of the main ophiolitic complex of the Wadi Ghadir mélange. (inset map in panel b shows the location of the study area in the Eastern Desert of Egypt).

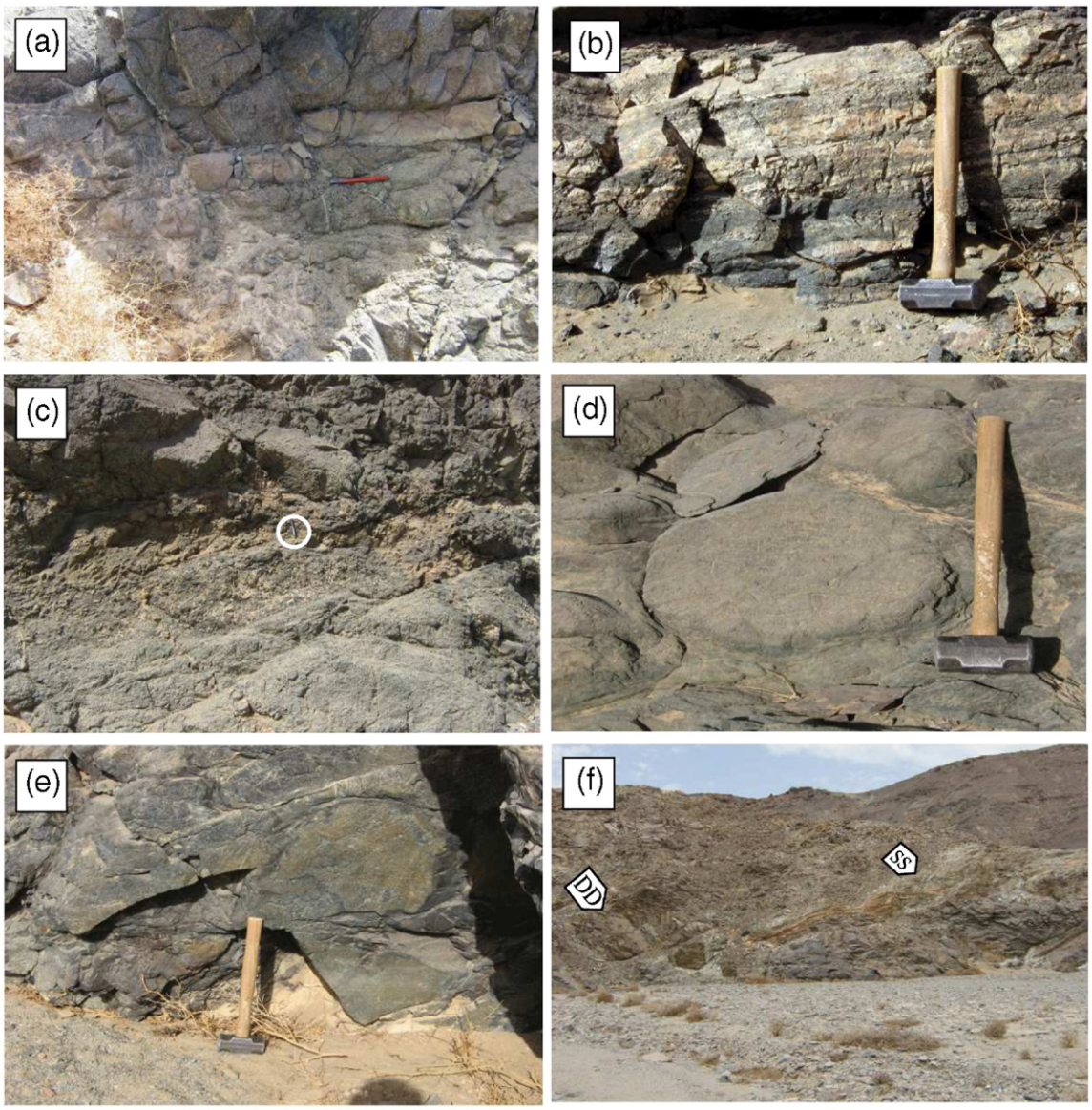

Fig. 2. Field photographs of ophiolitic block at Wadi Ghadir. (a) Offset granitic dike intruding ophiolitic gabbros at Wadi Saudi. (b) Sub-horizontal layering of alternating plagioclase-rich light bands and pyroxene-rich dark bands, layered gabbro unit at Wadi Saudi. (c) Isotropic gabbro unit at Wadi Saudi enclosing pocket of pegmatitic gabbro. (d) Oval pillow lavas of Wadi El Beda with concentric and radial fractures. (e) Porphyritic pillow lavas of Wadi Saudi rich in white patches of plagioclase phenocrysts. (f) Disrupted dike (DD) fragments within sheared serpentinite (SS) matrix of the Wadi Ghadir ophiolitic mélange in Wadi Beda.

El Beda is composed of tectonically imbricated blocks of gabbroic and volcanic rocks dipping to the southwest. Ultramafic mantle rocks are lacking in the ophiolite, but are widespread in the mélange as highly serpentinized blocks ranging from centimeters to kilometers in size, reaching up to mountain size as in Gebel Lawi and Gebel El Lewiwi. The Wadi Ghadir mélange is intruded by leucogabbros at Wadi El Beda and by different types of calc-alkaline granitoid plutons exposed in the eastern part of the Wadi Ghadir area (Fig. 2a; El Bayoumi, 1983).

Plutonic rocks of the WGO are composed of layered, coarse-grained massive and hypabyssal gabbros. Although they are structurally imbricated units, dipping moderately to the southwest, the layered gabbro is considered as the basal unit, transitional upward into the massive coarse-grained gabbro and the hypabyssal gabbro at the top. The basal gabbro is rhythmically layered with plagioclase-rich leuco-layers alternating with dark layers rich in altered pyroxene (Fig. 2b), both showing cumulate textures. The coarse-grained massive gabbro has a mottled appearance of rosette structure (Fig. 2c), which resulted from the irregular concentrations of dark altered pyroxene and light plagioclase crystals in adjacent spots. The massive gabbro displays horizontal shear zones with mylonitic and foliated fabrics. Hypabyssal gabbro has the same mineralogy but finer grain size than the other two types of gabbros. Some of these gabbro exposures show relict pyroxene and plagioclase phenocrysts. The gabbroic complex encloses large pods of pegmatitic gabbro and less common anorthosite, trondhjemite, and plagiogranite. The gabbroic complex is intruded by many diabasic dikes and sills. Their attitudes vary from sub-horizontal at the base, parallel to the layered gabbro, to sub-vertical near the top. Zircon dating of a plagiogranite revealed an age of 746 ± 19 Ma for the WGO (Kröner et al., 1992).

Pillow lavas are exposed at the northeastern end of Wadi El Beda and the eastern end of Wadi Saudi (Fig. 1c). The pillow lavas of Wadi El Beda extend for 400 m in length. They vary in shape, from circular to oval and in size from 20 cm to 1.5 m in diameter. Pillows, especially the larger ones, have massive green cores and vesicular margins (Fig. 2d). Pillow lavas are aphanitic, but plagioclase microphenocrysts are rarely visible. In Wadi Saudi pillow lavas extend laterally for about 70 m. In contrast to the vesicular pillow lavas of Wadi El Beda, pillow lavas in Wadi Saudi are plagiophyric and less vesicular (Fig. 2e).

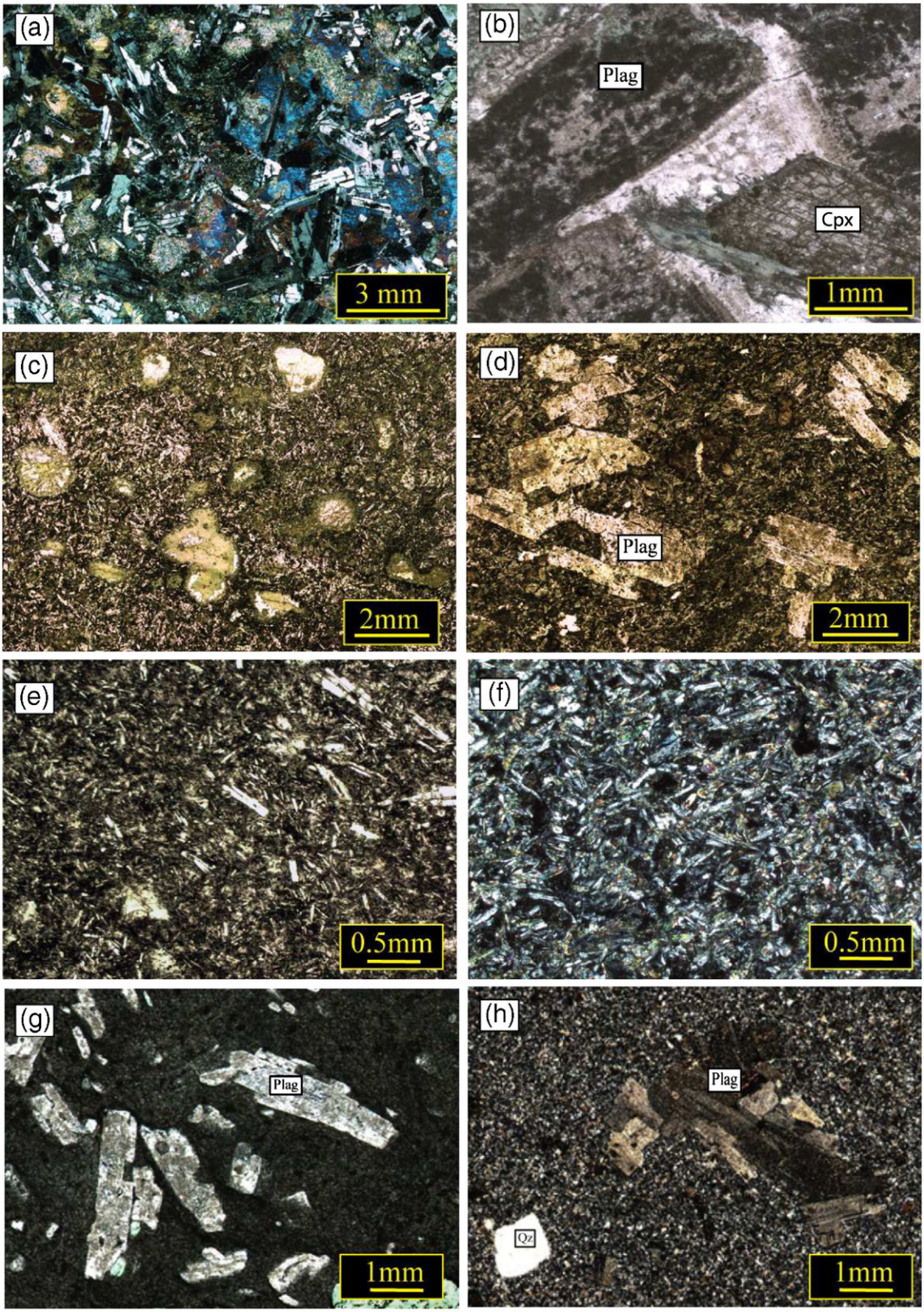

Fig. 3. Photomicrographs of ophiolitic rocks. (a) Ophitic and subophitic texture in gabbroic rocks. (XPL) (b) Rim alteration of pyroxene (Cpx) into green hornblende and fibrous actinolite and plagioclase (Plag) to albite, sericite and chlorite. (PPL) (c) Amygdaloidal pillow lavas, amygdales are filled with carbonate, actinolite and chlorite. (PPL) (d) Porphyritic texture and glomeroporphyritic texture formed by plagioclase phenocrysts. (PPL). (e) Basaltic dike with plagioclase microphenocryst. (PPL). (f) Doleritic dike with randomly oriented plagioclase laths and secondary amphiboles. (XPL). (g) Plagioclase phenocrysts in basaltic andesite (PPL). (h) Quartz (Qz) and plagioclase phenocrysts in dacite (XPL). XPL, crossed polarized light. PPL, plane polarized light.

Table 1
Measured and recommended major elements values for USGS standards DNC-1 and BIR-1.

Element	DNC-1		BIR-1	
	Measured	Recommended	Measured	Recommended
SiO_2	48.08	47	48.99	47.8
Al_2O_3	18.73	18.3	15.84	15.4
Fe_2O_3(T)	9.76	9.93	11.26	11.3
MnO	0.15	0.15	0.18	0.17
MgO	10.15	10.1	9.68	9.68
CaO	11.62	11.3	13.74	13.2
Na_2O	1.67	01.87	1.6	1.75
K_2O	0.27	0.23	0.09	0.03
TiO_2	0.49	0.48	0.99	0.96
P_2O_5	0.08	0.09	0.03	0.05

The mafic dikes are abundant in the area, cross-cutting the plutonic complex and the pillow lavas as individual dike swarms. The dikes intruding the gabbros vary in orientation, mainly striking NW–SE and NE–SW. In pillow lavas of Wadi El Beda, the dikes strike mostly NW–SE and dip SW. Some dikes cross-cutting the pillow lavas are folded, with fold axes plunging ~25° NW.

The rest of the Wadi Ghadir mélange is heterogeneous. Although the predominant blocks in the mélange are ophiolitic, blocks of talc-carbonate rocks, serpentinites, volcano-sedimentary and plutonic rocks are also common. The mélange also encloses highly disrupted dike swarms forming coherent massive blocks within the sheared mélange matrix (Fig. 2f). The block-to-matrix ratio of the WGM decreases towards the east. Farther to the west mafic and intermediate volcanic rocks occur as large blocks within a finer sedimentary matrix. To the north of the Hafafit gneissic dome, intermediate and felsic volcanic rocks crop out in a tuffaceous matrix, extending to Marsa Alam in the east. All volcanic rocks have been defined as a part of an island arc–back-arc complex in the Central Eastern Desert (Takla et al., 1990; Ramly et al., 1998; Hassanien, 2001).

3. Petrography

Different types of gabbros in the WGO share many petrographical features. They are composed generally of plagioclase and altered pyroxene. Gabbros have subophitic to ophitic texture (Fig. 3a). The crystallization sequence varies from olivine–plagioclase–clinopyroxene, which is the dominant order, to less common olivine–clinopyroxene–plagioclase. In cumulate gabbros, plagioclase and pyroxene represent the cumulus and intercumulus phases, respectively. Plagioclase laths are altered to epidote, albite, sericite and chlorite in order of decreasing abundance. The degree of albitization varies from intense pseudomorphic replacement to the development of chess-board albite rims around plagioclase laths. Augite is variably altered to hornblende (Fig. 3b). Some pyroxene crystals form coarse oikocrysts enclosing many plagioclase laths. Hornblende is altered further to fine aggregates of actinolite and chlorite. The space between plagioclase cumulate crystals is locally filled with secondary minerals such as actinolite, chlorite, epidote and calcite, and accessory minerals, such as opaque minerals, apatite and quartz. Plagioclase ranges from ~90% in leucocratic layers to ~20% in the melanocratic layers. Plagioclase laths, especially in the leucocratic layers, exhibit local alignment parallel to layer boundaries.

Pillow lavas in the WGO are divided into aphyric and porphyritic lavas, both of which are composed of altered plagioclase and ferromagnesian minerals. The ferromagnesian minerals are completely altered to hornblende, actinolite, and chlorite. The aphyric pillow lavas are rich in vesicles (20–30%) (Fig. 3c). The amygdales are filled with calcite, chlorite, quartz, actinolite, epidote, and/or biotite. Porphyritic pillow lavas have large plagioclase phenocrysts, up to 4 mm long (Fig. 3d), some of which display a glomeroporphyritic texture. Plagioclase phenocrysts are embedded in a microlitic groundmass composed of plagioclase, actinolite, chlorite, epidote, and titanite. The plagioclase phenocrysts are corroded and slightly altered to epidote, chlorite, carbonate, silica, and sericite. Vesicles are less common in the porphyritic pillows (<10%) and are filled with silica, carbonate, chlorite and epidote. Actinolite in the groundmass of both types of pillow lavas is altered to chlorite and epidote.

Dikes intruding the WGO are mainly basaltic and less commonly doleritic (Fig. 3e, f), and have a similar mineral assemblage of plagioclase, actinolite after pyroxene, epidote, chlorite and opaque minerals as in the pillow lavas. Basaltic dikes are aphyric to slightly porphyritic with coarser varieties showing subophitic textures. Plagioclase is zoned and is extensively epidotized, particularly in its core. Actinolite, chlorite, epidote and titanite are the main secondary minerals.

The doleritic and basaltic dikes in the WGM have almost the same petrography as the dikes in the WGO. Dioritic blocks are composed mainly of plagioclase and neomorphic biotite and accessory quartz. Chlorite, epidote and sericite are the main alteration minerals. To the north of Hafafit, the volcanic blocks range in composition from basalt to rhyolite. These volcanic rocks resemble the other arc metavolcanics of the Idfu-Marsa Alam Road described by Hassanien (2001). They are commonly porphyritic where the mafic and intermediate varieties have plagioclase and chloritized pyroxene and/or hornblende phenocrysts (Fig. 3g), and the felsic varieties have quartz and plagioclase phenocrysts (Fig. 3h).

4. Analytical methods

Rock samples were crushed, and then pulverized using an agate mill. Major elements and Sc were analyzed by Thermo Jarrell-Ash Enviro II ICP at ACTLABS in Ancaster, Canada. Samples were fused with a flux of lithium metaborate and lithium tetraborate in an induction furnace and then dissolved in 5% nitric acid containing an internal standard. Totals of major element oxides are 100 ± 1 wt.% and the analytical precisions for major elements are 1–2% and better than 5% for Sc. DNC-1 and BIR-1 were used as international reference standards to estimate accuracy of the major elements (Table 1).

Table 2
Measured and recommended values for USGS standards BHVO-1 and BHVO-2.

Element	BHVO-2 ($n=21$)		BHVO-1 ($n=11$)	
	Measured	Recommended	Measured	Recommended
Li	4.2	5.0	4.69	
V	313	317	321	
Cr	258	280	247	
Co	44	45	45	
Ni	155	119	150	
Cu	133	127	144	
Zn	110	103		
Rb	8.9	9.8	9.2	
Sr	382	389	390	
Y	22.8	26.0	23.3	28
Zr	156	172	165	179
Nb	14.32	18.00	14.9	19
Cs	0.10		0.11	0.13
Ba	128	130	128	139
La	14.70	15	14.78	16
Ce	36.69	38	37.01	39
Pr	5.18		5.13	5.4
Nd	23.76	25.0	23.40	25
Sm	5.90	6.20	5.83	6.4
Eu	1.98		1.97	2.06
Gd	6.23	6.30	6.20	6.4
Tb	0.89	0.90	0.91	0.96
Dy	5.1		5.10	5.2
Ho	0.94	1.04	0.95	0.99
Er	2.5		2.47	
Tm	0.32		0.31	0.33
Yb	1.92	2.00	1.88	2
Lu	0.26	0.28	0.26	0.29
Hf	4.23	4.10	4.52	4.4
Ta	0.9	1.04	0.86	1.2
Pb	2.58		4.18	2.6
Th	1.6	1.20	1.40	1.1
U	0.43		0.44	

Table 3
Major (wt.%) and trace elements (ppm) concentrations and significant element ratios for the ophiolitic rocks and associated dikes.

	Porphyritic pillows				Amygdaloidal pillows						Dikes D1				
	EGY-06-78	EGY-06-88	EGY-04-75	EGY-04-76	EGY-06-74	EGY-04-58	EGY-04-63	EGY-04-67	EGY-04-68	EGY-04-72	EGY-06-82	EGY-06-83	EGY-06-89	EGY-04-44	EGY-04-47
SiO_2	54.26	57.86	56.03	55.96	58.09	54.49	55.01	58.16	51.25	54.96	51.77	55.36	53.84	50.57	50.32
Al_2O_3	17.30	16.12	16.24	16.76	11.45	13.37	13.53	12.88	14.57	13.84	18.08	15.20	13.46	16.16	16.78
$Fe_2O_3^t$	10.95	7.74	10.08	9.98	8.60	11.60	12.28	10.80	14.15	11.72	8.28	9.06	14.74	9.52	11.99
MnO	0.13	0.11	0.14	0.13	0.21	0.19	0.22	0.18	0.21	0.18	0.14	0.17	0.22	0.14	0.18
MgO	2.31	2.36	2.13	2.10	1.89	2.57	2.73	2.24	3.08	3.63	7.03	7.11	3.44	8.32	6.30
CaO	6.61	5.70	7.29	6.58	12.65	8.75	8.19	7.59	8.50	7.03	9.93	6.86	6.62	10.01	8.45
Na2O	3.95	6.90	4.50	4.75	3.76	5.21	4.02	4.32	3.91	4.55	2.93	4.61	2.77	3.20	3.21
K2O	1.56	0.24	0.35	0.51	0.08	0.31	0.36	0.21	0.38	0.20	0.47	0.13	1.21	0.54	0.56
TiO2	2.29	2.40	2.64	2.65	2.98	3.23	3.37	3.31	3.64	3.52	1.20	1.35	3.15	1.33	1.97
P2O5	0.64	0.58	0.59	0.60	0.31	0.32	0.30	0.31	0.33	0.33	0.18	0.19	0.55	0.17	0.23
LOI	1.05	1.89	4.3	3.72	9.06	2.74	1.6	3.43	5.4	2.62	1.81	2.74	2.61	2.5	4.43
Mg-number	29.4	37.6	29.5	29.4	30.3	30.5	30.6	29.2	30.1	38.0	62.7	60.9	31.6	63.4	51.0
Cr	25	n.d.	33	33	14	59	n.d.	30	30	26	60	78	n.d.	306	60
Sc	26	21	26	26	33	38	40	39	42	41	26	31	35	34	31
V	158	137	164	160	337	431	430	415	459	452	186	207	327	211	155
Co	27	25	25	27	30	37	34	35	41	38	38	38	34	41	42
Ni	106	125	50	53	112	49	91	47	50	51	125	146	153	123	38
Rb	50.6	4.6	7.3	9.4	3.4	4.3	4.6	4.7	7.4	2.8	13.3	3.0	32.7	8.9	16.1
Cs	2.3	0.2	0.2	0.2	0.3	0.2	0.2	0.2	0.4	0.1	0.7	0.2	1.4	0.7	0.5
Ba	316	97	186	216	29	42	54	43	74	42	199	45	202	117	129
Sr	299	236	318	334	194	254	304	241	314	210	315	152	281	283	287
Pb	11.6	12.0	11.0	10.5	3.4	5.7	4.0	4.3	4.5	5.2	13.7	8.8	8.8	2.0	5.2
U	1.97	1.85	2.92	1.91	0.42	1.01	0.62	0.63	0.68	0.67	0.49	1.17	0.84	0.34	0.45
Th	7.48	6.80	7.00	6.77	1.42	2.02	1.99	1.76	1.90	1.92	1.40	2.66	2.37	0.87	1.31
Y	58.2	53.3	55.3	54.8	30.2	36.7	34.1	35.2	37.8	38.7	20.8	25.8	52.4	22.7	31.3
Zr	420	349	411	404	153	170	178	178	188	190	98	120	269	110	152
Ta	0.59	0.51	0.48	0.57	0.26	0.17	0.29	0.11	0.34	0.29	0.16	0.38	0.28	0.26	0.21
Nb	8.85	8.60	10.32	10.28	3.44	4.54	3.53	4.05	5.01	4.70	3.31	5.34	5.13	3.45	3.75
La	30.18	29.17	31.09	31.21	9.19	11.00	10.38	10.89	11.82	11.93	7.55	9.37	14.36	5.92	8.50
Ce	72.87	70.58	74.32	72.11	24.70	29.55	27.15	28.17	30.32	31.92	18.37	21.89	36.48	15.27	23.60
Pr	9.59	9.31	9.80	9.86	3.65	4.26	4.10	4.15	4.58	4.58	2.46	2.91	5.28	2.25	3.30
Nd	42.47	41.35	42.85	43.82	17.72	20.57	20.09	19.96	22.18	22.78	11.15	13.12	25.99	11.08	16.17
Sm	10.63	10.30	10.65	10.84	5.00	6.07	5.60	5.86	6.11	6.67	3.06	3.67	7.72	3.21	4.60
Eu	2.20	2.21	2.39	2.39	1.72	2.19	1.98	1.86	2.21	2.16	1.10	1.20	2.47	1.25	1.53
Gd	11.28	10.91	11.74	11.84	5.88	7.19	6.83	6.96	7.36	7.73	3.68	4.39	9.45	3.98	5.78
Tb	1.77	1.73	1.80	1.78	0.95	1.14	1.06	1.10	1.16	1.21	0.61	0.74	1.56	0.68	0.94
Dy	10.85	10.32	10.82	10.90	5.91	7.07	6.77	6.65	7.23	7.45	3.91	4.75	9.78	4.21	5.99
Ho	2.16	2.04	2.10	2.08	1.17	1.42	1.35	1.36	1.44	1.48	0.79	0.98	1.98	0.86	1.20
Er	6.28	5.77	5.73	5.79	3.34	4.01	3.91	3.76	3.98	4.25	2.33	2.88	5.69	2.48	3.49
Tm	0.85	0.75	0.73	0.71	0.44	0.54	0.54	0.49	0.55	0.56	0.32	0.40	0.77	0.34	0.51
Yb	5.31	4.57	4.16	4.14	2.72	3.35	3.37	3.12	3.34	3.22	2.06	2.56	4.87	2.23	2.98
Lu	0.75	0.61	0.55	0.51	0.36	0.46	0.49	0.41	0.44	0.42	0.30	0.37	0.69	0.30	0.43
Mo	0.4	0.3	1.4	1.4	0.1	1.1	0.5	0.8	0.4	0.3	0.3	3.4	0.4	0.3	0.4
Cu	19.5	76.6	32.6	175.3	15.4	14.1	20.4	10.4	28.5	12.5	64.5	51.7	41.8	61.0	28.9
Zn	114.2	129.5	109.8	105.6	59.9	105.1	108.8	82.5	104.8	112.3	91.4	2919.8	179.2	61.5	98.2
Ga	95.0	60.9	57.0	60.7	27.1	35.7	41.7	32.5	41.8	38.9	71.7	39.1	86.6	35.1	45.0
Al_2O_3/TiO_2	7.6	6.7	6.1	6.3	3.8	4.1	4.0	3.9	4.0	3.9	15.1	11.3	4.3	12.1	8.5
Nb/Y	0.15	0.16	0.19	0.19	0.11	0.12	0.10	0.12	0.13	0.12	0.16	0.21	0.10	0.15	0.12
La/Yb_{cn}	4.08	4.58	5.36	5.40	2.42	2.35	2.21	2.50	2.54	2.66	2.62	2.62	2.11	1.90	2.04
La/Sm_{cn}	1.83	1.83	1.88	1.86	1.19	1.17	1.20	1.20	1.25	1.15	1.59	1.65	1.20	1.19	1.19
Gd/Yb_{cn}	1.76	1.98	2.34	2.36	1.79	1.77	1.67	1.84	1.82	1.99	1.47	1.42	1.60	1.48	1.60
Eu/Eu*	0.61	0.64	0.63	0.65	0.97	0.99	0.98	0.89	1.00	0.92	1.00	0.91	0.89	1.03	0.91
Th/Yb	1.41	1.49	1.68	1.63	0.52	0.60	0.59	0.56	0.57	0.60	0.68	1.04	0.49	0.39	0.44
Th/Ce	0.103	0.096	0.094	0.094	0.057	0.068	0.073	0.062	0.063	0.060	0.076	0.122	0.065	0.057	0.056
Ce/Yb	14	15	18	17	9	9	8	9	9	10	9	9	7	7	8
Zr/Nb	47	41	40	39	44	37	50	44	38	40	30	22	52	32	40
Ti/Zr	33	41	39	39	117	114	114	112	116	111	73	67	70	72	78
Ba/La	10	3	6	7	3	4	5	4	6	4	26	5	14	20	15
V/Ti	0.012	0.010	0.010	0.010	0.019	0.022	0.021	0.021	0.021	0.021	0.026	0.026	0.017	0.026	0.013
Sc/Y	0.45	0.39	0.47	0.47	1.09	1.03	1.17	1.11	1.11	1.06	1.25	1.20	0.67	1.50	0.99
Latitude (N)	24° 46′ 0.3″	24° 46′ 17.2″	24° 46′ 38.93″	24° 46′ 38.90″	24° 45′ 44.5″	24° 45′ 46.84″	24° 45′ 54.94″	24° 45′ 44.82″	24° 45′ 44.39″	24° 45′ 46.76″	24° 46′ 17.3″	24° 46′ 16.3″	24° 46′ 16.6″	24° 46′ 19.24″	24° 46′ 06.56″
Longitude (E)	34° 53′ 29.9″	34° 53′ 12.3″	34° 53′ 10.54″	34° 53′ 10.52″	34° 53′ 22.1″	34° 53′ 32.24″	34° 53′ 29.65″	34° 53′ 29.11″	34° 53′ 28.10″	34° 53′ 26.27″	34° 53′ 44.4″	34° 53′ 25.4″	34° 53′ 8.6″	34° 53′ 43.80″	34° 53′ 42.83″

n.d. abbreviation for not detected.

(continued on next page)

Table 3 (*continued*)

					Dikes D2						Dikes D3				
EGY-04-48	EGY-04-50	EGY-04-52	EGY-04-59	EGY-04-66	EGY-06-73	EGY-04-45	EGY-04-54	EGY-04-55	EGY-04-69	EGY-04-70	EGY-06-86a	EGY-06-86b	EGY-06-84	EGY-06-87	EGY-04-62
51.50	49.95	50.28	47.95	48.05	57.27	57.63	56.13	56.14	58.27	59.57	48.53	48.89	50.30	49.87	48.51
17.84	16.91	16.22	18.93	17.07	16.83	16.22	16.99	16.93	16.13	16.52	17.33	18.01	13.86	15.43	17.71
8.64	12.20	12.73	10.33	10.99	6.89	6.91	7.90	7.83	6.75	7.56	8.61	8.23	15.51	12.80	9.65
0.14	0.18	0.19	0.15	0.14	0.11	0.10	0.12	0.12	0.11	0.10	0.14	0.14	0.25	0.20	0.15
6.95	6.38	6.42	7.77	9.06	4.94	4.56	4.93	5.04	4.69	2.85	10.07	9.92	4.37	5.76	8.90
9.61	8.58	7.85	9.62	10.04	8.20	6.82	8.28	8.15	7.24	4.47	11.28	10.78	8.24	9.51	10.45
3.34	3.09	3.22	3.20	2.63	4.29	6.05	3.88	3.99	5.29	6.09	2.15	1.90	3.63	2.73	2.63
0.64	0.43	0.66	0.46	0.31	0.26	0.38	0.42	0.43	0.31	1.27	0.76	0.99	0.14	0.94	0.47
1.23	1.98	2.17	1.39	1.53	1.05	1.13	1.18	1.19	1.02	1.38	1.05	1.06	3.38	2.49	1.40
0.15	0.24	0.25	0.19	0.19	0.15	0.18	0.19	0.17	0.14	0.21	0.07	0.08	0.37	0.28	0.13
2.87	4.67	4.5	4.78	4.2	1.58	1.28	2.91	3.1	2.01	2.73	4.04	4.11	2.5	2.39	3.49
61.4	50.9	50.0	59.9	62.0	58.7	56.7	55.3	56.1	57.9	42.8	69.9	70.5	35.8	47.1	64.7
243	63	56	69	558	42	118	35	44	126	22	68	75	n.d.	25	105
28	32	34	28	33	24	22	23	24	22	19	27	29	41	42	33
184	163	179	177	213	153	140	158	161	138	123	188	191	470	346	212
35	41	40	39	49	27	24	24	24	25	18	54	43	42	43	37
79	38	37	102	197	63	50	56	56	37	20	266	267	171	158	123
16.4	12.2	17.6	7.6	9.0	4.7	5.6	9.2	10.4	5.6	23.3	17.0	27.0	1.1	25.1	7.5
1.7	0.4	0.4	0.1	0.2	0.2	0.2	0.3	0.4	0.2	0.7	0.7	0.7	0.2	0.4	0.2
136	104	200	87	35	112	115	91	77	95	263	100	140	33	208	47
311	274	277	474	203	318	346	208	209	409	386	321	268	166	316	281
2.6	3.2	2.3	5.0	3.2	3.4	8.7	5.2	8.9	4.5	7.9	18.5	17.4	6.4	21.7	3.8
0.70	0.36	0.57	0.35	0.44	0.76	1.24	1.16	1.10	0.72	1.32	0.13	0.06	0.44	0.25	0.12
1.29	1.12	1.18	1.19	0.88	2.38	3.75	3.89	3.65	2.32	4.19	0.14	0.13	1.33	0.67	0.36
20.1	30.2	31.7	22.6	24.8	18.9	25.0	24.2	23.4	18.0	29.7	17.7	17.8	54.2	39.1	20.3
99	145	157	115	116	97	153	156	151	90	160	43	50	221	155	81
0.22	0.22	0.12	0.25	0.20	0.20	0.27	0.31	0.37	0.21	0.28	0.05	0.05	0.32	0.20	0.04
3.93	3.56	3.64	3.25	3.73	2.52	5.17	4.57	4.63	2.74	5.73	0.64	0.66	4.41	3.22	0.83
7.06	8.08	8.54	6.59	7.67	8.42	10.50	12.25	11.41	8.23	12.60	1.59	1.67	10.23	7.62	3.03
16.60	22.01	22.19	16.63	21.20	19.31	25.85	27.43	25.58	18.20	28.03	5.26	5.39	28.92	21.92	9.68
2.35	3.13	3.34	2.44	2.76	2.54	3.26	3.53	3.34	2.39	3.75	0.95	0.97	4.50	3.47	1.59
10.80	15.27	16.37	11.53	13.33	11.36	13.81	15.37	14.39	10.97	15.99	5.55	5.58	23.25	17.99	8.67
2.91	4.42	4.71	3.31	3.83	3.01	3.83	4.03	3.77	3.01	4.28	2.09	2.10	7.31	5.61	2.79
1.11	1.54	1.53	1.26	1.28	1.02	1.02	1.15	1.09	0.91	1.11	0.89	0.87	2.35	2.04	1.12
3.65	5.51	5.85	4.11	4.67	3.49	4.43	4.52	4.35	3.51	4.99	2.93	2.95	9.25	7.00	3.63
0.61	0.91	0.94	0.67	0.72	0.57	0.71	0.72	0.70	0.54	0.84	0.51	0.51	1.56	1.17	0.60
3.87	5.75	6.06	4.24	4.66	3.53	4.42	4.62	4.44	3.35	5.30	3.34	3.32	10.02	7.46	3.92
0.77	1.17	1.23	0.90	0.94	0.71	0.92	0.94	0.90	0.70	1.10	0.70	0.70	2.07	1.52	0.83
2.20	3.35	3.48	2.60	2.68	2.10	2.74	2.86	2.73	1.94	3.30	1.99	1.98	5.97	4.30	2.41
0.30	0.46	0.47	0.36	0.39	0.28	0.39	0.39	0.39	0.27	0.46	0.27	0.27	0.81	0.58	0.32
1.95	2.92	3.00	2.31	2.25	1.85	2.44	2.62	2.50	1.79	3.04	1.70	1.72	5.15	3.55	2.05
0.29	0.41	0.42	0.33	0.30	0.26	0.38	0.38	0.37	0.26	0.44	0.23	0.24	0.71	0.48	0.29
0.2	0.4	0.4	0.3	0.5	0.1	0.4	0.4	0.5	0.4	0.4	0.3	0.2	0.3	0.5	0.5
38.2	31.9	33.1	8.0	15.9	40.7	20.2	34.7	30.4	4.1	5.7	87.7	71.9	54.3	62.0	57.5
60.4	98.6	90.0	79.6	105.2	62.4	113.1	69.1	68.4	52.6	68.1	283.1	77.0	179.1	164.2	66.1
38.9	42.4	50.2	44.6	33.9	50.0	38.3	40.2	39.0	35.0	55.6	51.9	59.8	59.0	85.3	34.9
14.5	8.6	7.5	13.6	11.1	16.0	14.3	14.4	14.2	15.9	11.9	16.6	17.0	4.1	6.2	12.0
0.20	0.12	0.11	0.14	0.15	0.13	0.21	0.19	0.20	0.15	0.19	0.04	0.04	0.08	0.08	0.04
2.60	1.99	2.04	2.05	2.44	3.26	3.09	3.36	3.28	3.29	2.97	0.67	0.70	1.42	1.54	1.05
1.57	1.18	1.17	1.29	1.29	1.80	1.77	1.96	1.95	1.77	1.90	0.49	0.51	0.90	0.88	0.70
1.55	1.56	1.62	1.47	1.71	1.56	1.50	1.42	1.44	1.62	1.35	1.43	1.42	1.48	1.63	1.50
0.97	0.94	0.90	1.06	0.95	0.96	0.77	0.81	0.83	0.85	0.73	1.10	1.07	0.87	1.00	1.06
0.66	0.38	0.39	0.52	0.39	1.29	1.54	1.48	1.46	1.29	1.38	0.08	0.07	0.26	0.19	0.17
0.078	0.051	0.053	0.072	0.042	0.123	0.145	0.142	0.143	0.128	0.149	0.026	0.024	0.046	0.030	0.037
9	8	7	7	9	10	11	10	10	10	9	3	3	6	6	5
25	41	43	35	31	38	30	34	33	33	28	67	76	50	48	97
75	82	83	72	79	65	44	45	47	68	52	146	127	92	96	104
19	13	23	13	5	13	11	7	7	12	21	63	84	3	27	16
0.025	0.014	0.014	0.021	0.023	0.024	0.021	0.022	0.023	0.023	0.015	0.030	0.030	0.023	0.023	0.025
1.40	1.06	1.07	1.24	1.33	1.27	0.88	0.95	1.03	1.22	0.64	1.52	1.63	0.76	1.07	1.63
24° 46′	24° 46′	24° 46′	24° 45′	24° 45′	24° 45′	24° 46′	24° 46′	24° 46′	24° 45′	24° 45′	24° 46′	24° 46′	24° 46′	24° 46′	24° 45′
18.48″	03.50″	03.43″	46.84″	48.53″	39.1″	19.24″	00.77″	00.41″	43.42″	43.42″	17.2″	17.2″	16″	17.2″	54.94″
34° 53′	34° 53′	34° 53′	34° 53′	34° 53′	34° 53′	34° 53′	34° 53′	34° 53′	34° 53′	34° 53′	34° 53′	34° 53′	34° 53′	34° 53′	34° 53′
38.08″	45.92″	43.30″	32.24″	37.32″	26.3″	43.80″	41.46″	40.67″	26.77″	26.77″	12.3″	12.3″	6.2″	12.3″	29.65″

	Dikes D3				Dikes D4					Gabbros					
	EGY-04-61	EGY-04-65	EGY-04-77	EGY-04-78	EGY-06-61	EGY-06-79	EGY-04-46	EGY-04-49	EGY-04-74	EGY-04-42	EGY-04-43	EGY-04-51	EGY-04-57	EGY-06-80	EGY-06-81
SiO_2	48.82	48.82	48.68	48.91	56.97	53.29	54.92	55.12	52.54	48.78	47.14	48.55	50.58	46.07	47.38
Al_2O_3	17.50	14.56	17.56	17.71	17.50	19.34	15.44	16.51	17.62	16.90	18.68	14.45	15.62	16.50	17.13
$Fe_2O_3^t$	9.65	15.79	8.90	8.96	6.70	6.88	9.67	9.23	7.93	9.72	10.00	14.30	11.64	13.43	9.35
MnO	0.15	0.23	0.14	0.13	0.12	0.11	0.13	0.12	0.12	0.15	0.14	0.24	0.17	0.18	0.15
MgO	8.45	4.39	9.87	9.82	5.20	5.00	4.86	4.65	5.73	9.42	8.69	5.35	6.31	5.86	11.61
CaO	10.94	7.69	11.00	9.93	6.54	9.98	6.77	6.61	9.66	10.59	11.50	8.39	9.79	10.35	11.71
Na_2O	2.61	4.02	2.19	2.56	3.96	3.50	3.98	4.66	3.33	2.61	2.18	3.04	3.51	2.62	1.85
K_2O	0.29	0.22	0.53	0.79	2.07	0.47	1.67	1.03	1.28	0.76	0.26	0.78	0.39	1.14	0.16
TiO_2	1.45	3.27	1.07	1.05	0.73	1.20	1.92	1.66	1.38	1.03	1.18	4.53	1.82	3.75	0.63
P_2O_5	0.13	1.00	0.08	0.08	0.22	0.25	0.62	0.43	0.38	0.04	0.20	0.33	0.13	0.11	0.04
LOI	3.84	2.58	4	4.82	2.35	2.6	3.22	5.8	5.08	4.75	3.31	2.51	2.5	2.61	2.89
Mg-number	63.4	35.5	68.7	68.5	60.6	59.0	49.9	49.9	58.9	65.8	63.3	42.6	51.8	46.4	71.1
Cr	108	n.d.	324	328	28	44	141	100	42	86	133	n.d.	n.d.	n.d.	125
Sc	32	34	31	29	21	22	15	15	26	42	25	40	43	45	34
V	205	277	188	184	116	143	188	199	183	251	188	312	353	824	157
Co	40	27	40	44	23	28	30	27	23	44	38	32	34	40	53
Ni	145	83	218	227	44	79	56	52	61	116	156	124	66	166	215
Rb	12.8	9.3	11.6	22.1	58.1	12.7	32.2	24.8	20.7	20.1	4.2	19.6	9.1	32.6	5.5
Cs	0.2	0.2	0.7	0.5	0.5	0.3	0.5	0.7	0.7	0.5	0.5	0.2	0.6	1.2	0.5
Ba	48	83	76	99	274	134	522	350	332	94	59	157	71	157	39
Sr	332	299	288	337	383	462	685	666	621	326	205	215	220	419	195
Pb	36.9	3.6	2.4	2.2	4.5	4.6	5.4	7.1	12.1	2.4	2.0	3.6	2.4	8.4	10.8
U	0.13	0.39	1.48	0.12	1.09	0.75	1.12	1.17	0.68	0.05	0.07	0.45	0.21	0.12	0.07
Th	0.35	1.09	0.16	0.17	3.41	2.10	2.88	2.73	2.55	0.15	0.24	1.48	0.64	0.29	0.12
Y	20.3	47.4	18.3	17.8	24.6	18.2	17.9	14.9	15.0	10.0	13.1	31.1	23.9	16.0	8.3
Zr	80	385	48	50	146	143	204	141	122	18	33	128	80	43	18
Ta	0.07	0.26	0.05	0.05	0.35	0.27	0.41	0.33	0.27	0.03	0.06	0.27	0.11	0.11	0.02
Nb	0.86	3.27	0.74	0.73	5.65	4.89	8.91	5.81	4.44	0.31	0.61	3.26	1.37	1.38	0.29
La	2.99	9.10	1.62	1.71	19.54	12.84	23.45	20.59	16.82	0.88	2.24	7.20	3.90	2.43	0.88
Ce	9.37	27.24	5.09	5.31	43.43	28.46	54.84	46.76	37.12	2.63	6.25	18.81	10.69	6.58	2.62
Pr	1.58	4.61	0.97	0.97	5.31	3.54	7.44	6.32	4.73	0.47	1.03	2.88	1.72	1.09	0.43
Nd	8.51	24.75	5.61	5.64	22.01	15.07	32.29	27.76	19.32	2.79	5.58	14.65	9.01	5.97	2.51
Sm	2.81	7.61	2.20	2.12	5.06	3.51	6.72	5.67	3.83	1.15	1.89	4.49	3.06	2.13	0.95
Eu	1.09	2.69	0.95	0.87	1.34	1.23	1.89	1.65	1.23	0.61	0.84	1.71	1.33	1.09	0.57
Gd	3.71	9.58	3.08	2.92	5.06	3.70	6.03	4.78	3.74	1.68	2.54	5.91	4.16	2.94	1.37
Tb	0.62	1.52	0.51	0.50	0.78	0.58	0.76	0.59	0.52	0.28	0.41	0.95	0.71	0.49	0.24
Dy	3.94	9.36	3.50	3.34	4.68	3.47	3.94	3.33	3.06	1.92	2.53	6.00	4.59	3.16	1.57
Ho	0.82	1.88	0.70	0.68	0.92	0.69	0.69	0.57	0.60	0.39	0.52	1.23	0.96	0.64	0.33
Er	2.39	5.46	1.98	1.98	2.66	1.99	1.73	1.48	1.70	1.16	1.47	3.49	2.79	1.78	0.94
Tm	0.32	0.73	0.27	0.27	0.36	0.27	0.23	0.19	0.23	0.17	0.19	0.49	0.39	0.23	0.13
Yb	2.04	4.58	1.61	1.62	2.28	1.68	1.35	1.12	1.41	1.01	1.21	3.05	2.51	1.51	0.84
Lu	0.28	0.64	0.24	0.23	0.32	0.24	0.20	0.16	0.19	0.14	0.17	0.44	0.36	0.22	0.12
Mo	0.5	0.4	0.2	0.5	0.1	0.4	1.2	0.4	0.4	0.4	0.4	0.6	0.3	0.2	0.1
Cu	68.0	27.8	58.3	73.2	43.6	24.4	26.3	32.2	18.7	80.5	36.7	45.2	10.4	44.5	96.1
Zn	118.9	106.3	50.8	51.9	70.4	67.9	103.6	143.5	72.4	63.3	65.9	113.0	85.3	109.3	86.4
Ga	34.7	48.8	32.0	34.3	72.8	54.6	81.8	65.1	55.8	33.8	33.9	47.2	41.1	69.5	37.9
Al_2O_3/TiO_2	12.6	4.5	16.4	16.8	24.1	16.1	8.0	10.0	12.7	16.4	15.8	3.2	8.6	4.4	27.0
Nb/Y	0.04	0.07	0.04	0.04	0.23	0.27	0.50	0.39	0.30	0.03	0.05	0.10	0.06	0.09	0.03
La/Yb_{cn}	1.06	1.43	0.72	0.76	6.14	5.48	12.50	13.15	8.56	0.63	1.32	1.69	1.11	1.16	0.75
La/Sm_{cn}	0.7	0.77	0.48	0.52	2.50	2.36	2.25	2.34	2.83	0.49	0.77	1.03	0.82	0.74	0.60
Gd/Yb_{cn}	1.46	1.73	1.59	1.49	1.83	1.82	3.71	3.52	2.19	1.38	1.73	1.60	1.37	1.61	1.35
Eu/Eu*	1.08	0.97	1.06	1.06	0.81	1.05	0.93	0.93	1.01	1.35	1.17	1.02	1.14	1.34	1.53
Th/Yb	0.17	0.24	0.10	0.10	1.49	1.25	2.14	2.43	1.81	0.15	0.20	0.48	0.25	0.19	0.15
Th/Ce	0.037	0.040	0.031	0.031	0.078	0.074	0.053	0.058	0.069	0.057	0.038	0.079	0.060	0.044	0.048
Ce/Yb	5	6	3	3	19	17	41	42	26	3	5	6	4	4	3
Zr/Nb	93	118	65	69	26	29	23	24	27	58	54	39	58	31	62
Ti/Zr	109	51	134	126	30	50	57	71	68	343	215	212	136	523	211
Ba/La	16	9	47	58	14	10	22	17	20	107	26	22	18	65	45
V/Ti	0.024	0.014	0.029	0.029	0.027	0.020	0.016	0.020	0.022	0.041	0.027	0.011	0.032	0.037	0.041
Sc/Y	1.58	0.72	1.69	1.63	0.85	1.21	0.84	1.01	1.73	4.21	1.92	1.29	1.80	2.82	4.09
Latitude (N)	24° 45′ 54.94″	24° 45′ 48.53″	24° 46′ 17.11″	′24 °46′ 17.11″	24° 43′ 36.3″	24° 46′ 0.6″	24° 46′ 19.49″	24° 46′ 11.50″	24° 45′ 36.11″	24° 46′ 16.79″	24° 46′ 19.13″	24° 46′ 03.50″	24° 46′ 02.75″	24° 46′ 16.1″	24° 46′ 17″
Longitude (E)	34° 53′ 29.65″	34° 53′ 37.32″	34° 53′ 12.41″	34° 53′ 12.41″	34° 52′ 45.8″	34° 53′ 30″	34° 53′ 41.93″	34° 53′ 36.10″	34° 53′ 24.40″	34° 53′ 49.24″	34° 53′ 45.71″	34° 53′ 45.92″	34° 53′ 34.87″	34° 53′ 50.6″	34° 53′ 43″

Samples were analyzed for rare earth elements (REE), high field strength elements (HFSE), large ion lithophile elements (LILE) and transition metals (Ni, Co, Cr and V) by a high-sensitivity Thermo Elemental X7 ICP-MS in the Great Lakes Institute for Environmental Research (GLIER), University of Windsor, Canada, using the protocol of Jenner et al. (1990). Samples were dissolved in concentrated HF–HNO_3 mixture in screw-top Teflon (Savillex®) bombs for three days and further attacked with concentrated HNO_3–H_3BO_3–$H_2C_2O_4$ and then twice with 50% HNO_3. BHVO-1 and BHVO-2 were used as international reference standards to estimate accuracy of the measured trace elements (Table 2). Analytical precision is estimated as follow: 1–10% for REE, Rb, Sr, Ba, Y, Nb, Co, Cu, Zr, and U; 10–20% for V, Ni, Zn, Cs, Mo, and Ga; and 20–30% for Ta, Th, Cr, and Pb.

Major element analyses are calculated to 100 wt.% anhydrous basis. Mg-numbers were calculated as molar ratios of $[Mg^{2+}/(Mg^{2+}+Fe^{2+})]^{x}100$ after Ragland (1989). Chondrite (cn) and MORB compositions are derived from Sun and McDonough (1989), Pearce (1982) respectively. Europium (Eu/Eu*) anomalies were calculated with respect to neighboring REE (Rollinson, 1993).

5. Geochemical results

Whole-rock major and trace element data for the WGO are presented in Tables 3 and 4. The data for various mélange rocks are presented in Table 5. Sample "EGY-06-61" from the calc-alkaline leucogabbro, which crosscuts the mélange (Fig. 1b), is added to the D4 dikes columns of Table 3 for comparison. All rocks from the WGO and the mélange display basaltic to andesitic compositions (Fig. 4a). Blocks from the WGM are basaltic to andesitic, but blocks in the Hafafit mélange have a wider compositional range from basaltic to rhyolitic (Fig. 4c).

5.1. Gabbros

Gabbros of the WGO are tholeiitic (Fig. 4b). They have Mg-numbers between 43 and 71, and their SiO_2 content ranges from 46 to 51 wt.%. They have the lowest incompatible trace element (REE, Zr, Nb) contents of cogenetic rocks (Fig. 5). TiO_2, Fe_2O_3, and MgO display a large variation, but Al_2O_3, CaO and Na_2O are moderately variable (Table 3).

Chondrite-normalized REE patterns of the gabbros are variable (Fig. 6a). The samples with the highest Mg-number show convex upward, light rare earth element- (LREE-) depleted patterns with $La/Yb_{cn}=0.63$ and $La/Sm_{cn}=0.49$. With decreasing Mg-number, REE patterns become flat and then slightly enriched in LREE. The sample with the lowest Mg-number has $La/Yb_{cn}=1.69$ and $La/Sm_{cn}=1.03$. The less evolved sample has a positive Eu anomaly which decreases with an increase in the overall abundance of REE. The absolute abundances of REE in the gabbroic rocks vary as samples with low Mg-numbers have higher total REE contents than samples with higher Mg-numbers.

MORB-normalized trace element patterns of the gabbroic rocks are enriched in LILE (Sr, K, Rb, Ba, Th) relative to HFSE (Nb, Ta, Zr, Ti, Y) and HREE and show negative Nb and Ta anomalies (Fig. 7a). The gabbroic rocks are slightly enriched in LILE, up to 10× MORB values, and the less evolved samples are slightly depleted in HFSE and REE compared to MORB (Fig. 7a). Values of the transition metals, Sc and Cr are close to MORB values.

5.2. Pillow lavas

Pillow lava samples are composed predominantly of basaltic andesites and andesites (Fig. 4a). They have the lowest Mg-numbers (29–38) of all rock types in the WGO. Pillow lavas of Wadi El Beda (amygdaloidal pillows) plot in the tholeiitic field, whereas the pillow lavas of Wadi Saudi (porphyritic pillows) plot in the calc-alkaline field (Fig. 4c). Porphyritic pillows have higher Al_2O_3, CaO, and Na_2O but lower Fe_2O_3, MgO, and TiO_2 than amygdaloidal pillows. Porphyritic pillows are more enriched in Zr (349–441 ppm) and other incompatible elements relative to amygdaloidal pillows (Fig. 5).

Both porphyritic and amygdaloidal pillow lavas have similar chondrite-normalized REE patterns (Fig. 6b). They are both enriched in LREE, but the porphyritic pillows are more fractionated ($La/Yb_{cn}=4.1$–5.4 and $La/Sm_{cn}=1.8$–1.9) than the amygdaloidal pillows ($La/Yb_{cn}=2.2$–2.7 and $La/Sm_{cn}=1.2$–1.3). The porphyritic pillows show negative Eu anomalies ($Eu/Eu^*=0.61$–0.65). Both pillow lava types are enriched in LILE, HFSE and REE relative to MORB (Fig. 7b).

5.3. Dikes

Although dikes cutting the WGO show little change in their petrography, their chemical compositions display a large variation. They plot in tholeiitic (D1 dikes, D3 dikes), transitional (D2 dikes) and

Table 4
Summary of major (wt.%) and trace (ppm) elements concentrations and significant element ratios for the Wadi Ghadir ophiolitic complex and associated dikes.

	Porphyritic pillow	Amygdaloidal pillow	Dikes D1	Dikes D2	Dikes 3	Dikes 4	Gabbros
SiO_2	54.3–57.9	51.3–58.2	48.1–55.4	56.1–59.6	48.5–50.3	52.5–56.97	46.1–50.6
Al_2O_3	16.1–17.3	11.5–14.6	13.5–18.9	16.1–17.0	13.9–18.0	15.4–19.34	14.5–18.7
$Fe_2O_3^t$	7.7–11.0	8.6–14.2	8.3–14.7	6.8–7.9	8.23–15.79	6.7–9.7	9.4–14.3
MgO	2.4	1.9–3.6	3.4–9.1	2.9–5.0	4.4–10.1	4.7–5.7	5.4–11.6
CaO	5.7–7.3	7.0–12.7	6.6–10.0	4.5–8.3	7.7–11.3	6.5–10.0	8.4–11.7
TiO_2	2.29–2.65	2.98–3.64	1.20–3.15	1.02–1.38	1.05–3.38	0.73–1.92	0.63–4.53
Mg-number	29.4–37.6	29.2–30.6	31.6–63.4	42.8–58.7	35.5–70.5	49.9–60.6	42.6–71.1
Cr	25–33	14–59	56–557	21–126	25.–328	28–140	n.d.–133
Sc	21–26	33–42	26–35	19–24	27–42	15–26	25–45
V	137–164	337–459	155–327	123–161	184–470	116–199	157–824
Co	25–27	30–41	34–49	18–27	27–44	23–30	32–44
Ni	50–125	47–112	37–197	20–63	83–267	44–79	66–215
Th	6.77–7.48	1.42–2.02	0.87–2.66	2.32–4.19	0.13–1.33	2.55–3.41	0.12–1.48
Y	54.8–55.3	30.2–38.7	20.1–52.4	18.1–29.7	17.7–54.2	14.9–24.6	8.3–31.1
Zr	349–411	153–190	98–269	90–160	43–385	122–204	18–128
Nb	8.6–10.32	3.44–5.01	3.31–5.34	2.52–5.73	0.64–4.41	4.44–8.91	0.29–3.26
La	29.17–31.21	9.19–11.93	5.92–14.36	8.23–12.60	1.59–10.23	12.84–23.45	0.88–7.20
Nd	41.35–43.82	17.72–22.78	10.80–25.99	10.97–15.99	5.55–24.75	15.07–32.29	2.51–14.65
Sm	10.30–10.84	5.00–6.67	2.90–7.72	3.01–4.26	2.09–7.61	3.51–6.72	0.95–5.91
Gd	10.97–11.84	5.88–7.73	3.65–9.45	3.49–4.99	2.92–9.58	3.70–6.03	1.37–5.91
Yb	4.14–5.31	2.72–3.37	1.95–4.87	1.79–3.04	1.61–5.15	1.12–2.28	0.84–3.05
La/Yb_{cn}	4.08–5.40	2.21–2.66	1.90–2.62	2.97–3.36	0.67–1.54	5.48–13.15	0.63–1.69
La/Sm_{cn}	1.83–1.88	1.15–1.25	1.17–1.65	1.77–1.97	0.48–0.9	2.25–2.83	0.49–1.03
Gd/Yb_{cn}	1.76–2.36	1.67–1.99	1.42–1.71	1.35–1.62	1.42–1.73	1.82–3.71	1.35–1.75
Eu/Eu*	0.61–0.65	0.89–1.00	0.89–1.06	0.73–0.96	0.87–1.10	0.81–1.05	1.02–1.53

Table 5
Major (wt.%) and trace elements (ppm) concentrations and significant element ratios for ophiolitic mélange fragments and associated fragmented dikes.

	Ghadir Mélange				Fragmented Dikes in Ghadir Mélange											Hafafit Mélange						
	EGY-06-62	EGY-06-63	EGY-06-64	EGY-06-65	EGY-06-85	EGY-06-75	EGY-06-90	EGY-06-91	EGY-06-66	EGY-06-67	EGY-06-68	EGY-06-69	EGY-06-70	EGY-06-71	EGY-06-72	EGY-04-34	EGY-04-35	EGY-04-36	EGY-04-37	EGY-04-38	EGY-04-39	EGY-04-40
SiO_2	55.84	57.58	50.21	52.02	49.80	50.92	50.09	57.21	50.96	50.07	53.25	49.61	47.69	53.60	52.71	56.73	75.63	56.47	52.06	69.60	60.81	50.87
Al_2O_3	18.36	15.81	14.38	15.48	18.39	14.10	18.28	15.22	18.10	16.17	13.33	17.00	15.54	14.21	16.02	15.53	13.67	19.19	20.30	14.06	14.55	17.90
$Fe_2O_3^t$	5.58	8.28	14.23	11.06	9.07	14.44	9.36	12.09	8.78	9.00	14.95	9.34	13.25	13.23	10.43	7.55	1.69	7.53	9.01	4.55	7.98	12.64
MnO	0.09	0.09	0.23	0.16	0.15	0.22	0.15	0.22	0.13	0.14	0.23	0.15	0.21	0.20	0.17	0.10	0.03	0.12	0.14	0.06	0.14	0.19
MgO	6.07	3.92	4.67	5.62	7.76	4.13	7.93	1.99	5.65	9.46	3.36	8.64	6.86	3.60	5.56	6.55	0.29	3.24	5.14	2.27	3.77	4.73
CaO	6.91	6.14	8.86	8.68	9.35	8.16	8.97	5.95	10.69	9.70	6.63	10.59	9.94	7.46	9.11	4.77	1.51	6.97	7.21	2.09	7.85	4.52
Na_2O	4.88	5.08	3.67	4.20	2.52	4.36	2.63	4.25	3.10	2.81	3.35	2.76	2.95	3.15	3.44	5.86	5.60	3.86	4.59	3.49	2.77	2.59
K_2O	0.42	0.69	0.47	0.38	1.40	0.39	1.04	0.70	0.64	0.86	1.49	0.35	0.71	1.23	0.60	1.22	1.31	1.51	0.23	2.99	1.23	3.59
TiO_2	1.52	1.78	2.94	2.31	1.40	2.89	1.39	1.55	1.67	1.44	2.91	1.41	2.53	2.85	1.75	1.26	0.20	0.88	1.08	0.56	0.62	2.67
P_2O_5	0.34	0.62	0.33	0.09	0.17	0.38	0.18	0.81	0.30	0.35	0.49	0.15	0.31	0.48	0.23	0.44	0.08	0.21	0.23	0.34	0.26	0.31
LOI	1.61	2.15	0.52	1.07	3.88	1.43	3.77	0.62	1.23	1.82	0.77	2.16	2	1.24	1.81	3.5	2.4	9.9	5.49	3.94	6.8	5.33
Mg-number	68.3	48.4	39.4	50.2	62.9	36.2	62.7	24.6	56.1	67.5	30.9	64.7	50.7	35.0	51.4	63.2	25.3	46.1	53.1	49.8	48.3	42.6
Cr	28	47	27	49	64	12	64	n.d.	69	136	17	98	50	16	27	512	405	356	377	422	31	n.d.
Sc	17	13	39	43	28	37	29	20	28	30	38	35	41	34	35	18	2	14	20	10	29	31
V	116	171	422	343	170	393	175	36	192	202	321	212	314	320	249	134	8	89	134	110	230	169
Co	22	25	42	41	37	39	41	17	36	43	36	47	49	33	38	29	2	24	28	11	19	32
Ni	90	101	141	126	94	130	101	72	133	236	120	133	149	118	76	193	31	82	85	42	31	74
Rb	8.8	11.8	7.5	8.4	39.8	7.5	25.9	20.0	17.1	19.9	54.6	9.5	16.2	40.7	12.0	20.2	51.6	36.2	3.1	60.6	21.7	52.6
Cs	0.2	0.6	0.1	0.3	0.6	0.5	0.2	3.6	0.6	0.8	1.9	0.6	0.6	1.8	0.3	0.4	1.1	0.9	0.8	0.5	0.3	0.5
Ba	200	281	80	97	280	53	85	200	158	269	257	163	91	179	131	417	201	376	111	434	283	502
Sr	545	1269	214	249	480	196	407	371	403	511	292	367	325	265	298	392	175	369	576	193	486	284
Pb	6.0	8.8	2.4	5.0	18.6	3.2	5.3	7.2	3.1	4.2	3.9	2.9	3.1	4.0	3.2	43.4	74.2	28.1	113.5	215.9	3.3	2.1
U	2.10	0.89	0.42	0.85	0.16	0.63	0.14	0.73	0.69	0.65	0.73	0.26	0.17	0.75	0.54	6.23	6.80	0.55	0.48	1.78	0.76	0.55
Th	4.31	3.22	1.29	2.62	0.38	1.85	0.37	2.08	2.22	2.47	2.38	0.91	0.65	2.06	1.93	4.82	19.71	1.37	1.21	6.72	3.58	1.48
Y	21.6	14.4	52.8	38.7	21.1	53.5	21.9	59.3	28.1	21.2	54.4	24.9	36.5	46.4	28.5	22.1	22.3	18.9	18.0	14.2	12.1	33.7
Zr	271	191	202	297	100	203	109	275	178	153	236	131	188	214	135	234	171	105	113	186	108	201
Ta	0.53	0.24	0.26	0.32	0.12	0.32	0.12	0.53	0.31	0.42	0.37	0.16	0.21	0.41	0.22	0.46	2.71	0.22	0.19	0.36	0.22	0.42
Nb	6.95	5.47	3.56	3.80	1.70	4.12	1.71	7.59	4.32	6.49	4.99	2.45	2.74	5.19	3.22	6.46	20.49	2.49	2.35	5.45	4.71	5.12
La	18.15	29.13	9.04	10.61	4.57	11.10	4.89	14.50	10.59	15.91	14.15	5.95	7.70	13.39	8.48	24.85	34.42	9.06	9.10	40.94	20.85	10.23
Ce	44.60	68.32	25.16	28.56	13.10	29.70	13.75	43.98	29.04	36.88	35.96	16.74	23.36	33.52	21.40	55.35	68.42	21.27	21.34	85.03	46.28	26.01
Pr	5.59	8.92	4.05	4.03	2.03	4.54	2.13	6.34	4.09	4.76	5.21	2.56	3.72	4.87	3.05	6.93	7.62	2.95	2.86	10.39	6.00	3.91

(*continued on next page*)

Table 5 (*continued*)

	Ghadir Mélange				Fragmented Dikes in Ghadir Mélange											Hafafit Mélange						
	EGY-06-62	EGY-06-63	EGY-06-64	EGY-06-65	EGY-06-85	EGY-06-75	EGY-06-90	EGY-06-91	EGY-06-66	EGY-06-67	EGY-06-68	EGY-06-69	EGY-06-70	EGY-06-71	EGY-06-72	EGY-04-34	EGY-04-35	EGY-04-36	EGY-04-37	EGY-04-38	EGY-04-39	EGY-04-40
Nd	23.34	37.83	20.96	18.22	10.29	22.90	10.79	31.90	19.19	20.06	25.79	12.70	18.89	23.64	14.58	28.78	27.97	12.91	12.51	41.05	25.23	19.15
Sm	5.19	7.25	6.72	5.13	3.07	7.14	3.21	9.30	5.06	4.47	7.69	3.74	5.63	6.90	4.19	5.91	5.53	3.34	3.35	7.41	5.03	5.40
Eu	1.55	2.15	2.32	1.63	1.18	2.43	1.18	3.36	1.58	1.45	2.55	1.35	2.00	2.24	1.44	1.45	0.80	1.15	1.34	1.53	1.30	1.66
Gd	4.93	5.40	8.76	6.04	3.83	8.99	4.00	11.13	5.57	4.48	9.64	4.54	6.81	8.43	5.05	5.77	4.87	3.72	3.35	5.39	4.11	6.49
Tb	0.73	0.66	1.48	1.07	0.63	1.53	0.66	1.79	0.88	0.68	1.59	0.75	1.12	1.37	0.84	0.76	0.71	0.59	0.52	0.57	0.47	1.04
Dy	4.32	3.25	9.59	6.98	4.03	9.80	4.21	11.12	5.39	4.10	10.05	4.70	6.99	8.68	5.37	4.26	4.07	3.50	3.47	2.80	2.48	6.48
Ho	0.84	0.55	1.99	1.46	0.82	2.00	0.85	2.25	1.07	0.81	2.04	0.95	1.40	1.76	1.09	0.88	0.77	0.71	0.70	0.51	0.47	1.33
Er	2.42	1.45	5.82	4.42	2.32	5.85	2.40	6.37	3.08	2.35	5.93	2.75	4.01	5.10	3.20	2.54	2.34	2.18	2.01	1.50	1.33	3.88
Tm	0.33	0.16	0.81	0.63	0.31	0.80	0.32	0.86	0.42	0.31	0.81	0.38	0.54	0.69	0.44	0.33	0.31	0.32	0.29	0.20	0.18	0.53
Yb	2.11	0.90	5.24	4.23	1.93	5.11	1.97	5.43	2.68	2.01	5.22	2.40	3.39	4.35	2.83	2.14	2.14	2.10	1.79	1.29	1.14	3.45
Lu	0.31	0.12	0.76	0.62	0.26	0.71	0.26	0.79	0.39	0.29	0.75	0.34	0.48	0.63	0.41	0.32	0.31	0.32	0.30	0.49	0.18	0.51
Mo	0.3	0.2	1.2	0.2	0.2	0.6	0.3	0.8	0.2	0.1	0.5	0.2	0.4	0.6	0.2	0.9	0.8	1.7	1.2	1.4	0.6	0.5
Cu	13.85	34.66	38.61	44.08	35.63	34.98	38.74	27.97	20.70	23.23	28.08	53.60	55.32	39.95	32.65	71.52	5.51	42.08	41.63	116.59	90.65	24.68
Zn	58.8	112.2	544.8	100.9	103.1	145.9	88.7	167.7	73.4	81.9	134.2	68.8	101.6	120.1	82.1	133.3	103.1	105.5	118.2	210.4	67.5	104.1
Ga	67.2	79.7	55.2	56.0	85.5	54.4	54.1	92.0	59.5	69.2	81.0	54.5	52.7	66.8	55.4	66.5	59.3	70.6	49.2	57.0	50.3	77.1
Al_2O_3/TiO_2	12.1	8.9	4.9	6.7	13.1	4.9	13.2	9.8	10.8	11.3	4.6	12.0	6.1	5.0	9.2	12.3	69.4	21.8	18.7	25.1	23.3	6.7
Nb/Y	0.32	0.38	0.07	0.10	0.08	0.08	0.08	0.13	0.15	0.31	0.09	0.10	0.07	0.11	0.11	0.29	0.92	0.13	0.13	0.38	0.39	0.15
La/Yb_{cn}	6.17	23.23	1.24	1.80	1.70	1.56	1.78	1.91	2.83	5.67	1.94	1.78	1.63	2.21	2.15	8.33	11.52	3.10	3.65	22.78	13.10	2.13
La/Sm_{cn}	2.26	2.59	0.87	1.33	0.96	1.00	0.98	1.01	1.35	2.30	1.19	1.03	0.88	1.25	1.31	2.71	4.01	1.75	1.76	3.57	2.68	1.22
Gd/Yb_{cn}	1.94	4.97	1.38	1.18	1.64	1.45	1.68	1.69	1.72	1.84	1.53	1.56	1.66	1.60	1.48	2.23	1.88	1.47	1.55	3.46	2.98	1.56
Eu/Eu*	0.94	1.05	0.93	0.89	1.06	0.93	1.01	1.01	0.91	0.99	0.91	1.00	0.99	0.90	0.96	0.76	0.47	1.00	1.23	0.74	0.87	0.86
Th/Yb	2.05	3.58	0.25	0.62	0.20	0.36	0.19	0.38	0.83	1.23	0.46	0.38	0.19	0.47	0.68	2.25	9.20	0.65	0.67	5.21	3.14	0.43
Th/Ce	0.097	0.047	0.051	0.092	0.029	0.062	0.027	0.047	0.077	0.067	0.066	0.054	0.028	0.061	0.090	0.087	0.288	0.064	0.057	0.079	0.077	0.057
Ce/Yb	21	76	5	7	7	6	7	8	11	18	7	7	7	8	8	26	32	10	12	66	41	8
Zr/Nb	39	35	57	78	59	49	64	36	41	24	47	53	69	41	42	36	8	42	48	34	23	39
Ti/Zr	34	56	87	47	84	85	76	34	56	56	74	65	81	80	78	32	7	50	58	18	35	80
Ba/La	11	10	9	9	61	5	17	14	15	17	18	27	12	13	15	17	6	42	12	11	14	49
V/Ti	0.013	0.016	0.024	0.025	0.020	0.023	0.021	0.004	0.019	0.023	0.018	0.025	0.021	0.019	0.024	0.018	0.007	0.017	0.021	0.033	0.062	0.011
Sc/Y	0.79	0.90	0.74	1.11	1.33	0.69	1.33	0.34	1.00	1.42	0.70	1.41	1.12	0.73	1.23	0.81	0.09	0.74	1.11	0.70	2.39	0.92
Latitude (N)	24° 44′ 22.7″	24° 44′ 22.7″	24° 44′ 22.7″	24°44′ 23.7″	24° 46′ 16.8″	24° 45′ 40.1″	24° 46′ 16.6″	24° 48′ 42.8″	24° 44′ 27.7″	24° 44′ 36.4″	24° 44′ 42.3″	24° 44′ 42.3″	24° 44′ 55.5″	24°45′ 24.2″	24° 45′ 31″	24° 57′ 27″	24° 56′ 58.81″	24° 57′ 33.75″	24° 57′ 34.85″	25° 03′ 20.56″	25° 03′ 38.7″	25° 03′ 38.41″
Longitude (E)	34° 52′ 46.6″	34° 52′ 46.6″	34° 52′ 46.6″	34°52′ 47.3″	34° 53′ 14.1″	34° 53′ 30.2″	34° 53′ 8.6″	34° 50′ 51.5″	34° 52′ 49.7″	34° 52′ 54.2″	34° 52′ 58.3″	34° 52′ 58.3″	34° 53′ 5.1″	34° 53′ 9.5″	34° 53′ 8.8″	34° 31′ 50.63″	34° 33′ 34.81″	34° 33′ 20.34″	34° 33′ 19.58″	34° 49′ 12.5″	34° 48′ 42.41″	34° 48′ 34.85″

n.d. abbreviation for not detected.

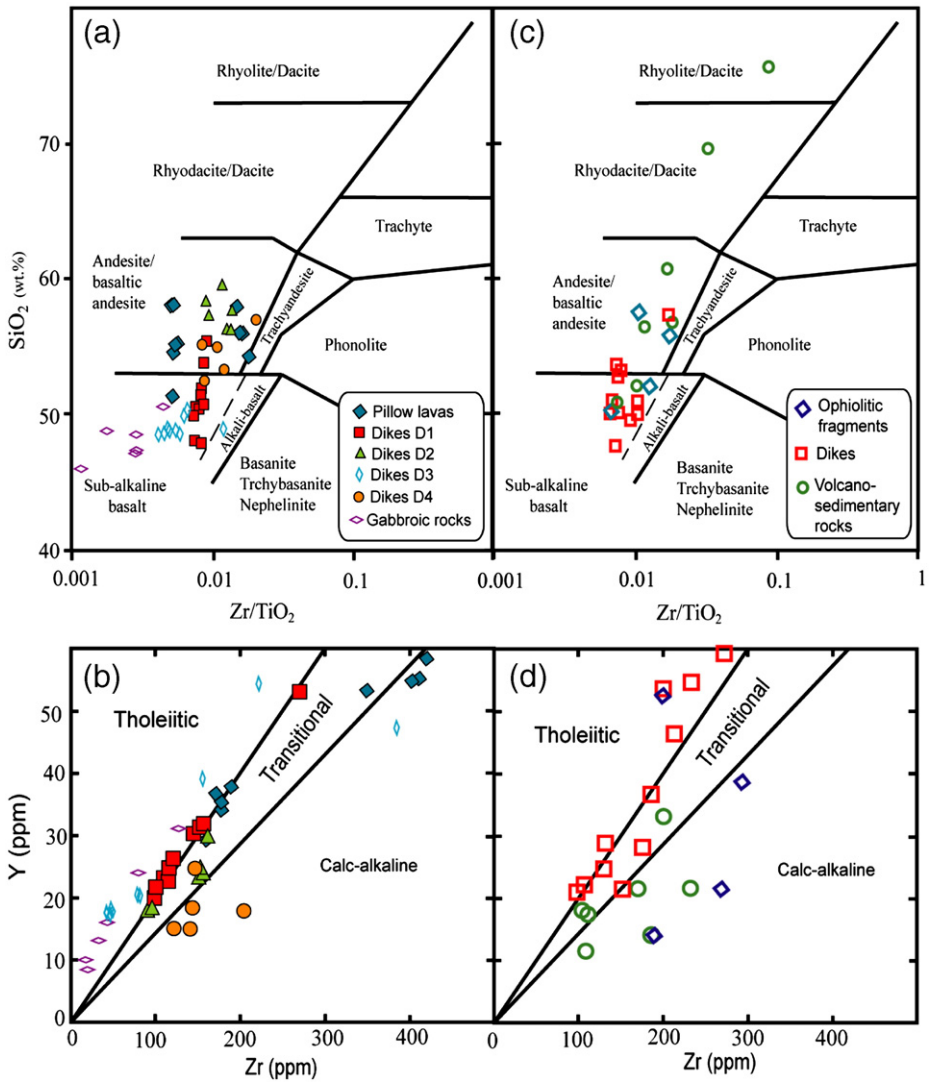

Fig. 4. Zr/TiO_2 versus SiO_2 diagram of Winchester and Floyd (1977) for (a) Wadi Ghadir ophiolite complex and for (b) Wadi Ghadir ophiolitic mélange and island arc fragments. Zr versus Y diagram of Barrett and MacLean (1994) to distinguish the magma series of (c) the Wadi Ghadir ophiolite complex and of (d) the Wadi Ghadir ophiolitic mélange and island arc fragments.

calc-alkaline (D4 dikes) fields (Fig. 4b). Their Mg-numbers ranging from 31 to 70 and greatly overlap with, but are generally higher than, those of the pillow lavas.

Chondrite-normalized REE patterns of different generations of dikes show some variations. Tholeiitic dikes have both LREE-depleted chondrite-normalized patterns (D3 dikes) and slightly LREE-enriched patterns (D1 dikes) (Fig. 6c, d). LREE-depleted samples have La/Yb_{cn} ranging between 0.8 and 1.5 and La/Sm_{cn} between 0.5 and 0.9 with convex-upward patterns, similar to the less fractionated gabbros. The other tholeiitic series is LREE-enriched ($La/Yb_{cn} = 1.9–2.6$ and $La/Sm_{cn} = 1.2–1.7$). Rare earth element patterns of D1 dikes are similar to those of the amygdaloidal pillow lavas.

Dikes of the transitional series (D2) have Mg-numbers ranging between 43 and 59, and Zr contents in the range of 90 to 160 ppm. Chondrite-normalized REE patterns of D2 dikes are enriched in LREE with $La/Yb_{cn} = 3.0–3.4$ and $La/Sm_{cn} = 1.8–2.0$ (Fig. 6e). Their patterns are similar to those of the porphyritic pillow lavas, and they also exhibit negative Eu anomalies ($Eu/Eu^* = 0.73–0.96$). Calc-alkaline dikes (D4) have Mg-number ranging between 50 and 61 and Zr contents between 122 and 204 ppm. The chondrite-normalized REE patterns of D4 dikes show strong LREE enrichment with La/Yb_{cn} between 5.5 and 13.2 (Fig. 6f).

The tholeiitic dikes show minor variations in their trace-element patterns. D3 dikes are slightly depleted in HFSE and REE relative to MORB (Fig. 7c), but D1 dikes have HFSE contents close to MORB values (Fig. 7d). Transition metal contents of both groups are variable relative to MORB. The patterns of D2 dikes are characterized by a Th peak similar to the porphyritic pillow lavas (Fig. 7e).

MORB-normalized trace element patterns of D4 dikes are characterized by enrichment in highly incompatible elements LILE, LREE and HFSE over HREE (Fig. 7f). These rocks are highly enriched in LILE in comparison to MORB ($\geq 10\times$ MORB) but are depleted in HREE relative to MORB. Compared to the other types of rocks in the study area, D4 dikes have the highest contents of the most incompatible trace elements and the most fractionated REE patterns.

5.4. Ophiolitic mélange

The blocks in the ophiolitic mélange along Wadi El Beda show much variation in lithology and chemistry. Their chemical affinities range from tholeiitic to calc-alkaline (Fig. 4d). The diorite sample (EGY6-06-63) has the highest SiO_2 and Na_2O but the lowest MgO and CaO contents compared to other basaltic and doleritic rocks in the mélange. The basaltic fragments have near-flat chondrite-normalized REE patterns,

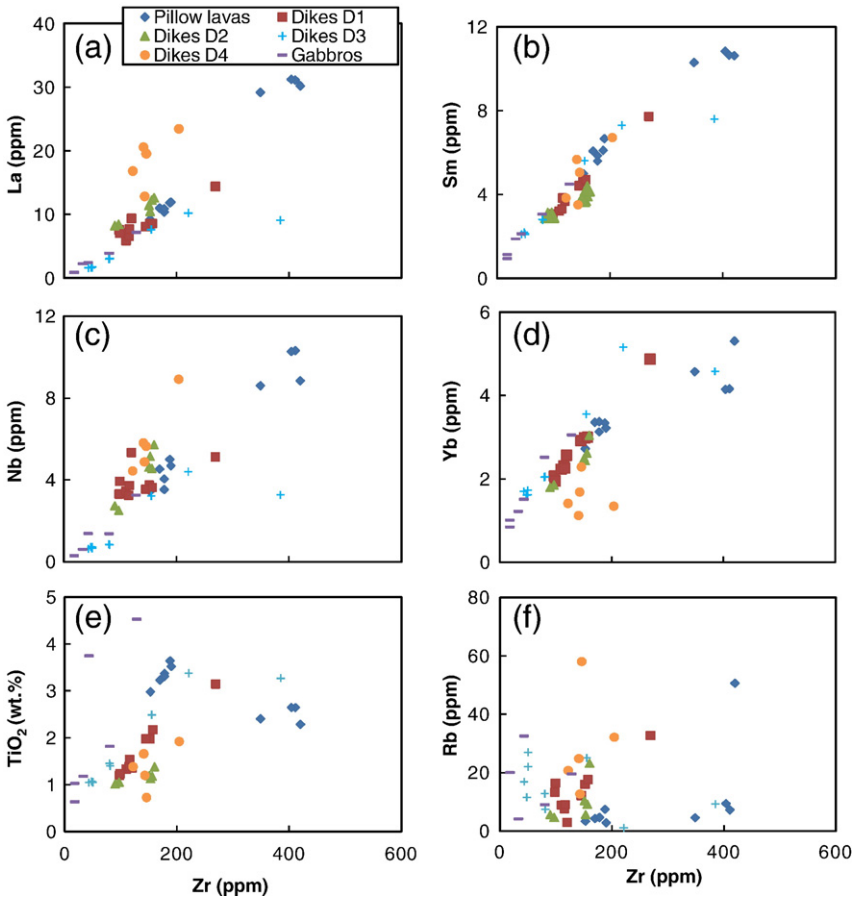

Fig. 5. Variation diagrams of Zr versus (a) La, (b) Sm, (c) Nb, (d) Yb, (e) TiO_2, (f) Rb for the Wadi Ghadir ophiolitic complex and associated dikes.

La/Yb_{cn} = 1.2–1.8 and La/Sm_{cn} = 0.9–1.3, whereas the intermediate igneous rocks have LREE-enriched patterns, La/Yb_{cn} = 6.2–23.2 and La/Sm_{cn} = 2.3–2.6 (Fig. 8a). All mélange units are characterized by negative Nb and Ta anomalies and enrichment in LILE over HFSE (Fig. 8b, d, f). Blocks of dikes within the Wadi El Beda ophiolitic mélange are made of tholeiitic basalt (Fig. 4c, d) which show consistent chondrite-normalized REE patterns that are flat to slightly LREE-enriched, La/Yb_{cn} = 1.6–5.7 and La/Sm_{cn} = 0.9–2.3 (Fig. 8c). As are other blocks in the mélange, the dikes are characterized by enrichment in LILE over HFSE and have negative Nb and Ta anomalies (Fig. 8d).

To the north of the Hafafit gneissic dome, the volcanic blocks in the mélange range in composition from basalt to rhyolite with transitional to calc-alkaline affinity (Fig. 4c, d). These rocks are enriched in LREE and LILE over HFSE where their degree of enrichment is higher than the rest of the blocks in the Wadi Ghadir ophiolitic mélange (Fig. 8). The ratios of La/Yb_{cn} and La/Sm_{cn} range from 2.1 to 22.8 and from 1.2 to 3.8, respectively. These rocks are also characterized by negative Nb, Ta, Ti and Eu anomalies (Fig. 8f).

6. Discussion

6.1. Alteration process and element mobility

Although the WGO rocks preserve their original igneous textures, they show textural evidence for extensive alteration and metamorphic overprint. Metamorphism and alteration of ophiolitic rocks resulted mainly from oceanic hydrothermal processes (Gillis and Banerjee, 2000). Static alteration is common in the gabbroic rocks during the first phase of metamorphism as evidenced by the replacement of primary pyroxene, (augite) by hornblende. Subsequently, the gabbros and the volcanic rocks were altered hydrothermally to an assemblage of actinolite, albite, chlorite, epidote, and titanite under greenschist-facies conditions. Accretion-related dynamic metamorphism mainly affected the mélange matrix, reaching greenschist-facies conditions.

To assess the alteration effect on the original chemistry of the WGO, we adopted the alteration criteria of Polat et al. (2002) and Polat and Hofmann (2003). All samples loss of ignition (LOI) values less than 6 wt.%, suggesting that the rocks have not been highly altered. The consistency of REE patterns of the Wadi Ghadir rocks and lack of Ce anomalies suggest that the concentrations of these elements were not modified significantly, and that they reflect their magmatic concentrations (Fig. 6).

Large ion lithophile elements (LILE) are expected to be mobile under most alteration conditions, but most major elements, high field strength elements (HFSE), REE) and transitional metals are expected to be immobile under most metamorphic conditions (Winchester and Floyd, 1976; Dostal et al., 1980; Humphries, 1984; Polat and Hofmann, 2003). Due to this differential mobility, HFSE and REE (but not LILE) show a good correlation with the least mobile element, Zr, on binary diagrams for the WGO (Fig. 5).

Blocks in the ophiolitic mélange are expected to be more altered than the main WGO due to the intensive deformation which they experienced. The degree of alteration in the mélange is difficult to evaluate because of the heterogeneous nature of various rocks making up the blocks. But for the blocks of dikes within the WGM, the high mobility of the LILE relative to REE and HFSE can be detected through their MORB-normalized patterns (Fig. 8b, e). The same conclusion can be reached through the normalized patterns of the arc rocks exposed north of the Hafafit gneissic dome (Fig. 8f).

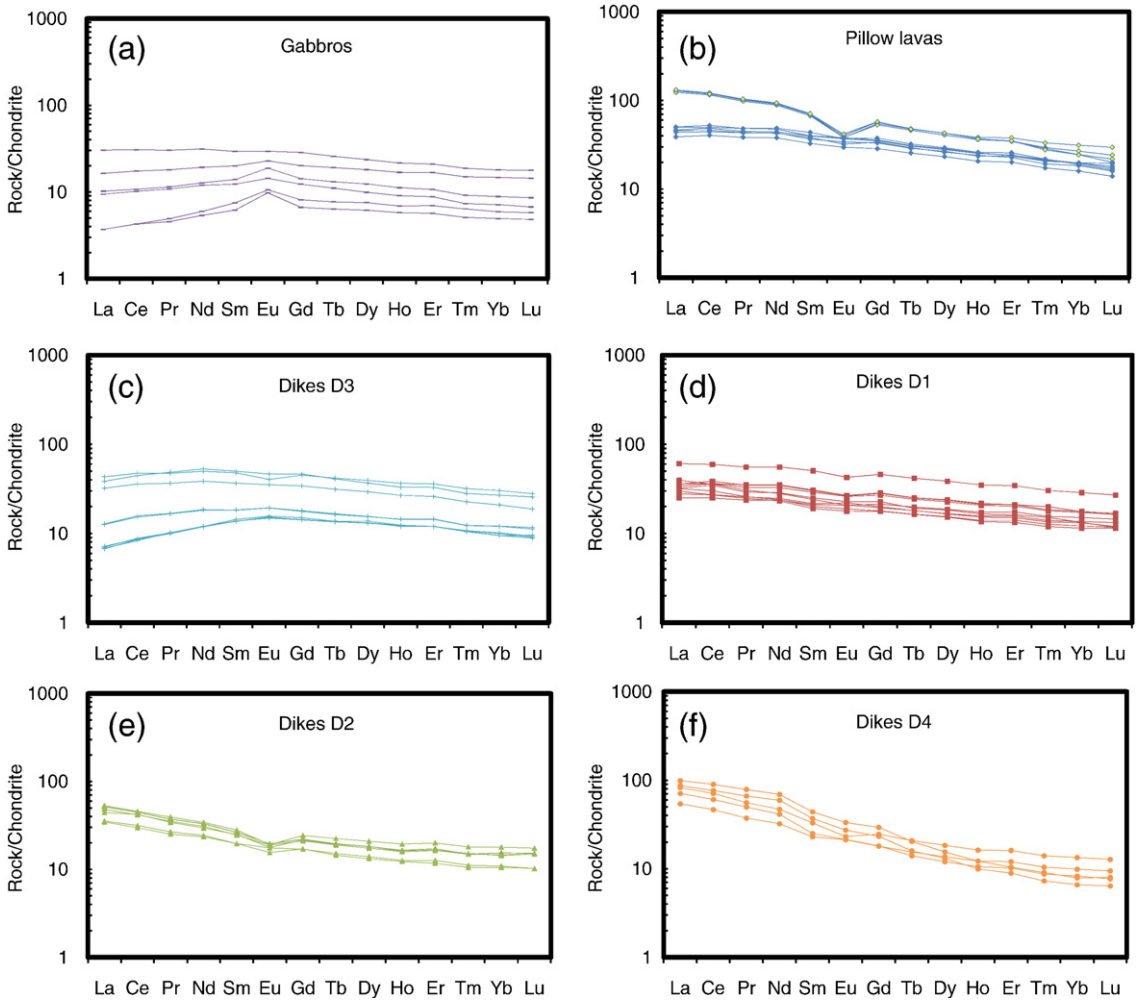

Fig. 6. Chondrite-normalized REE patterns for, (a) Gabbros, (b) Pillow lavas; solid yellow symbols for porphyritic pillows, (c) D3 dikes, (d) D1 dikes, (e) D2 dikes, and (f) D4 dikes (normalizing chondrite values from Sun and McDonough, 1989).

6.2. Mantle source characteristics

All samples analyzed for this study have consistent MORB-normalized trace element patterns characterized by enrichment of LILE relative to HFSE thus creating negative Nb and Ta anomalies. Such geochemical characteristics are consistent with magma compositions generated in supra-subduction zone settings and are attributed to mantle wedge melting affected by fluid released from a subducted slab (Pearce, 1982; Tatsumi and Kogiso, 2003). Enrichment in LILE stems from the mobility of these elements during slab dehydration (Pearce and Peate, 1995). High-field strength elements behave in a conservative way during subduction, and so their concentration in the rocks reflects their concentration in the mantle wedge (Pearce, 2008). To discriminate between the relative contribution of a mantle source and a subduction component, Pearce (1983) and Pearce and Peate (1995) developed plots using M/Yb versus Nb(Ta)/Yb, where M is the incompatible element of interest (Fig. 9). On these diagrams, subduction-related enrichment of element (M) results in displacement from the mantle array, which is defined by mantle-derived oceanic basalts.

For Zr and Y, all rock types of the Wadi Ghadir area form linear trends overlapping with the mantle array (Fig. 9a, b). These values pass through the values of MORB and below OIB, indicating that HFSE and HREE were not important components in the subduction flux. Light REE (La) and MREE (Sm) plots are still confined to the mantle array but slightly moved towards the upper boundary (Fig. 9c, d). D4 dikes plot above the upper boundary of the mantle array. These features collectively suggest that LREE and, to some extent MREE, were added to the mantle wedge from the subducted slab but not in significant amounts except for D4 dikes that were highly affected by fluxes from the subducted slab and/or the sub-continental lithospheric mantle. Large ion lithophile elements (U and Th) form linear trends that are sub-parallel to, but are displaced above, the mantle array towards higher U/Yb and Th/Yb ratios (Fig. 9e, f). These higher ratios indicate high contributions of these elements from a subduction component.

The behavior of some elements, conservative or non-conservative, is dependent on the nature of contributions from the subducted slab to the mantle wedge, either in fluid or in melt. Zirconium is one of these elements (Pearce and Peate, 1995). Zirconium plots in the mantle array thus indicating a minor role of sediments or sediment melting during the petrogenesis of these rocks. The limited contribution from subducted sediments to the mantle wedge is detected also through the tendency of the samples towards higher Ba/La ratios rather than higher Th/Yb (Class et al., 2000; Woodhead et al., 2001) and the relatively low Th/Ce ratios (<0.1) (Hawkesworth et al., 1997) (Table 3). As the sediment input to the mantle wedge is limited, all samples, except D4 dikes, follow the low Ce/Yb trend of Hawkesworth et al. (1993) (Fig. 10). The blocks in the Wadi Ghadir ophiolitic mélange have low Th/Ce ratios and relatively higher Ba/La ratios than Th/Yb (Table 3).

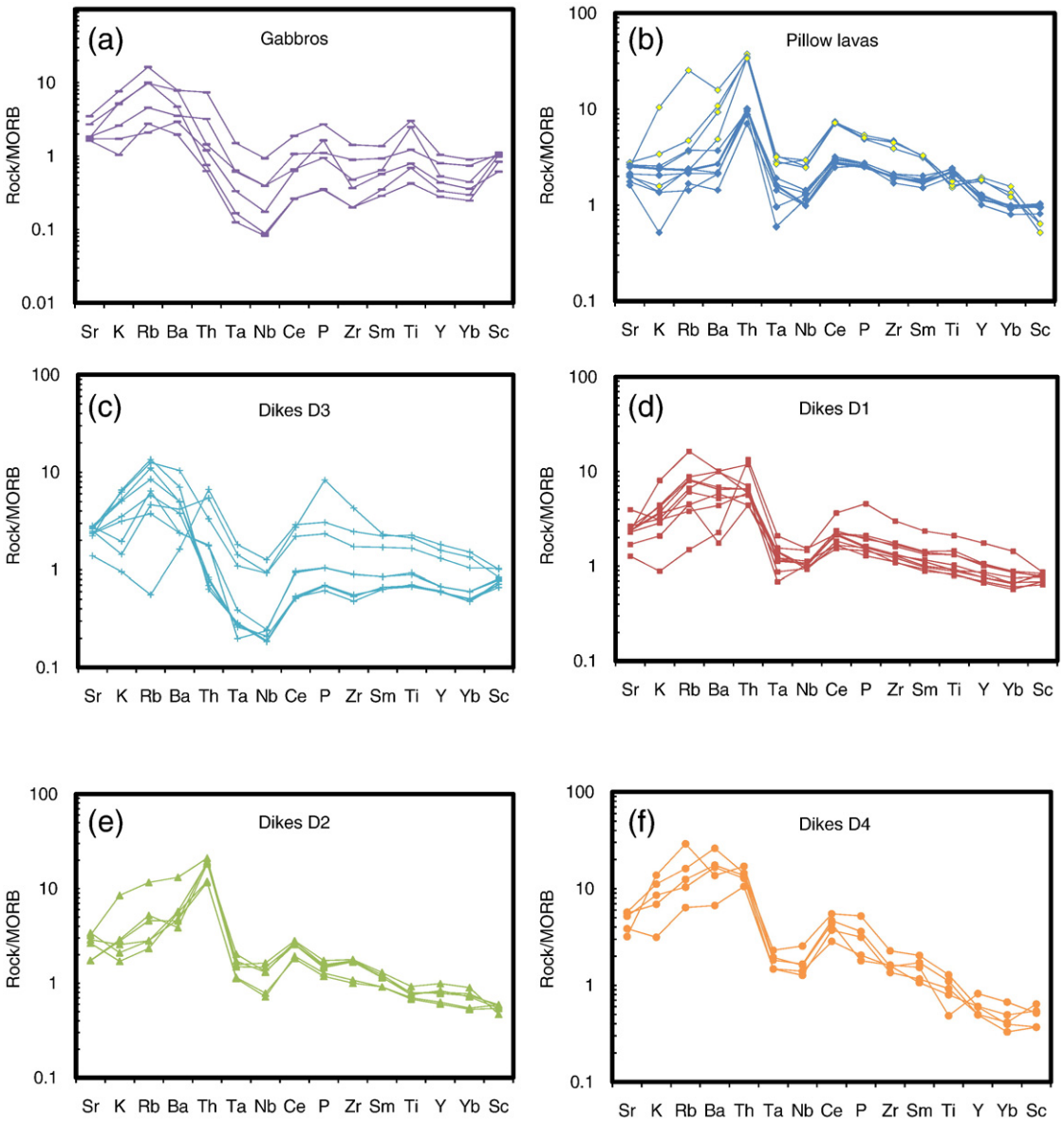

Fig. 7. MORB-normalized trace elements patterns for, (a) Gabbros, (b) Pillow lavas; solid yellow symbols for porphyritic pillows, (c) D3 dikes, (d) D1 dikes, (e) D2 dikes, and (f) D4 dikes. Symbols as in Fig. 6. (normalizing MORB-values after Pearce, 1982).

As they are less affected by the subduction-related fluxes, conservative elements can be used to evaluate the composition of the mantle wedge, and their ratios are useful in assessing the mantle wedge composition without being affected by pooled and fractional partial melting or fractional crystallization (Pearce and Peate, 1995). On M/Yb versus Nb/Yb diagrams (Fig. 9), where M is a conservative element, our data plot along the mantle array where D3 dikes and gabbroic rocks extend to the depleted MORB end whereas the rest cluster around average MORB. Melting of a slightly depleted mantle source is consistent with high Zr/Nb in the gabbroic rocks (31–62) and D3 dikes (48–118) compared to an average N-MORB ratio (~32). D4 dikes extend to the enriched end of the mantle array but not to OIB values, and this is consistent with their lower Zr/Nb (23–29) than average MORB. Other dike groups, D1 and D2, along with porphyritic and amygdaloidal pillow lavas, have Zr/Nb ratios ranging from 22 to 52 with values closer to average MORB on the mantle array. Blocks of dikes in the WGM have Zr/Nb ratios (25–64) close to the range of D1 and D2 dikes and pillow lavas. We infer that magmas of both WGO and the disrupted dikes in the mélange may have been derived from the same mantle source.

Variations in trace element patterns and in Zr/Nb ratios of the analyzed samples indicate either mantle heterogeneity and/or selective tapping of the mantle column in a dynamic melting model (Pearce et al., 1995). Variations in La/Sm_{cn} relative to Sm suggest that the gabbroic rocks and D1, D2, D3, and D4 dikes may be the products of heterogeneous mantle and/or dynamic melting. Porphyritic lavas and D2 dikes and amygdaloidal lavas and D1 dikes may be genetically related, however, through fractional crystallization processes (Fig. 11).

The elevated Gd/Yb_{cn} ratio (>1) of the WGO indicates that the mantle source was at a depth of garnet stability. The garnet signature in these rocks may have resulted from melting of garnet peridotite, which is stable at a depth >90 km (OIB source), melting of a garnet pyroxenite/spinel peridotite source (N-MORB source) (cf. Hirschmann and Stolper, 1996), or addition of subduction-related melts in equilibrium with garnet eclogite (cf. Kessel et al., 2005). Calc-alkaline dikes (D4) have the highest Gd/Yb_{cn} ratio (2.2–3.7). On the La/Yb versus Yb diagram of

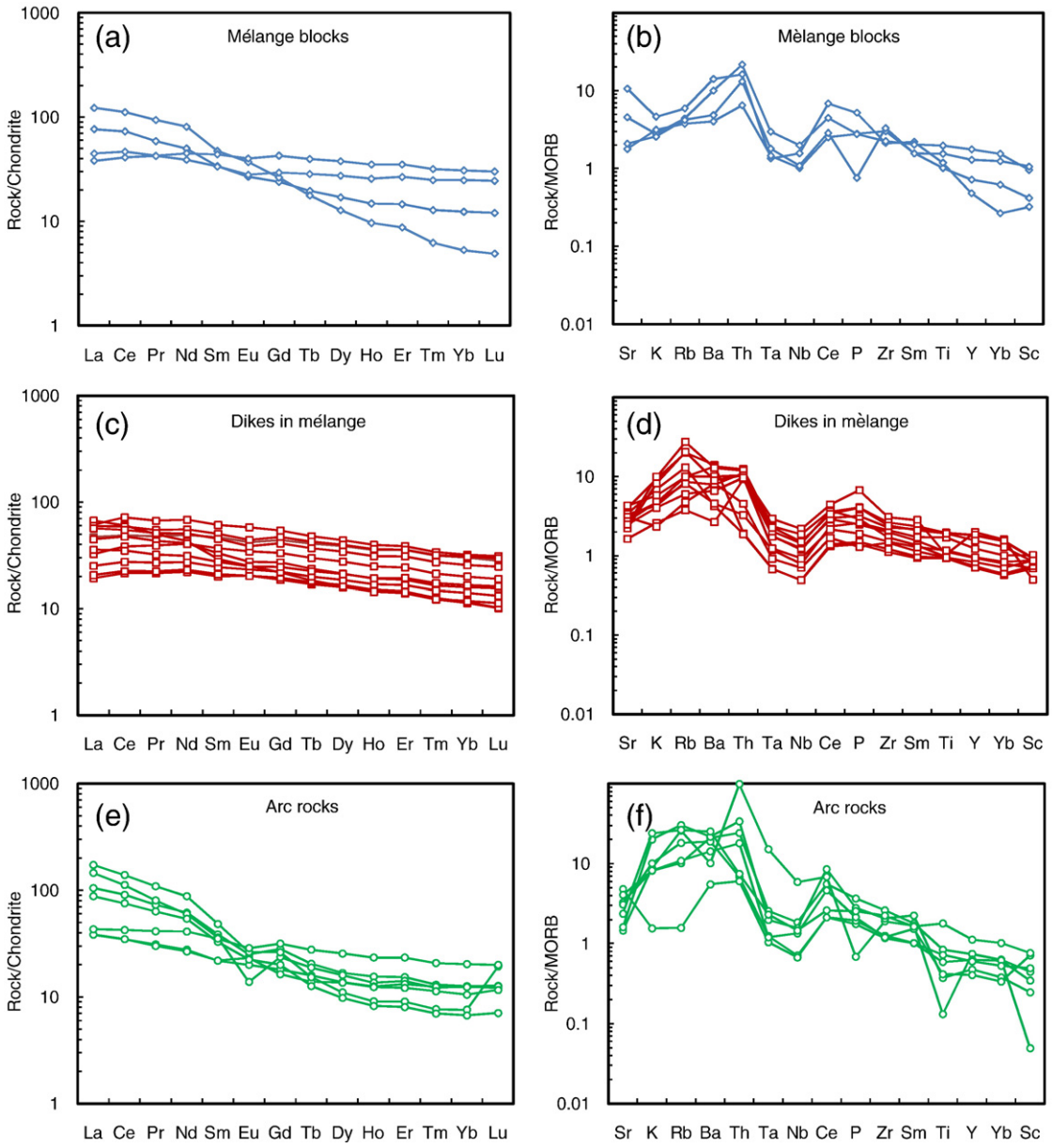

Fig. 8. (a) Chondrite-normalized REE patterns for the Wadi Ghadir mélange blocks, (b) MORB-normalized trace element patterns for the Wadi Ghadir mélange blocks, (c) Chondrite-normalized REE patterns for fragmented dikes in the Wadi Ghadir ophiolitic mélange, (d) MORB-normalized trace elements patterns for fragmented dikes in the Wadi Ghadir ophiolitic mélange, (e) Chondrite-normalized REE patterns for arc rocks north of Hafafi and northwest the Wadi Ghadir ophiolitic mélange, (f) MORB-normalized trace element patterns for arc rocks north of Hafafi and northwest the Wadi Ghadir ophiolitic mélange (chondrite and MORB values after Sun and McDonough (1989) and Pearce (1982) respectively).

Baker et al. (1997), the analyzed samples plot close to the spinel lherzolite trend except for D4 dikes that extend along the garnet lherzolite melting curve (Fig. 12). This may indicate derivation of the magmas of D4 dikes from a deeper source or at least mixing of their magmas with melt from a garnet lherzolite source. However, the other samples have lower Yb contents at the same MgO contents indicating the generation of their melts from a shallower spinel lherzolite mantle, which may have been veined by garnet pyroxenite.

6.3. Tectonic setting and geodynamic evolution

Although a complete Penrose-type sequence is absent in the WGO, its gabbroic rocks and pillow lavas are interpreted as remnants of Neoproterozoic oceanic crust (El Sharkawy and El Bayoumi, 1979; El Bayoumi, 1980, 1983; Kröner et al., 1992; Farahat et al., 2004). Normal-MORB-normalized patterns of these ophiolitic rocks along with D1, D2, and D3 dikes are consistent with the evolution of the WGO in a supra-subduction zone geodynamic setting (cf. Pearce, 1982, 2003; Pearce et al., 1984).

The ophiolitic rocks and associated D1, D2, and D3 dikes of the Wadi Ghadir area have high average abundances of incompatible HFSE and Y and low ratios of Ti/Zr, V/Ti, and Sc/Yb (Table 3). These features characterize melting of a normal MORB mantle source beneath back-arc basin spreading centres (Woodhead et al., 1993). The systematic compositional variations in the WGO rocks are analogous to the compositional variations observed from in-situ oceanic crust of modern back-arc basins such as the Manus Basin (Sinton et al., 2003). The compositional variations of back-arc-related rocks can be attributed to source heterogeneity beneath back-arc basins that resulted from variable mixing of fertile mantle, melt-depleted mantle and slab-derived components (Martinez and Taylor, 2003). The chemistry of the mantle wedge is affected by fluids derived

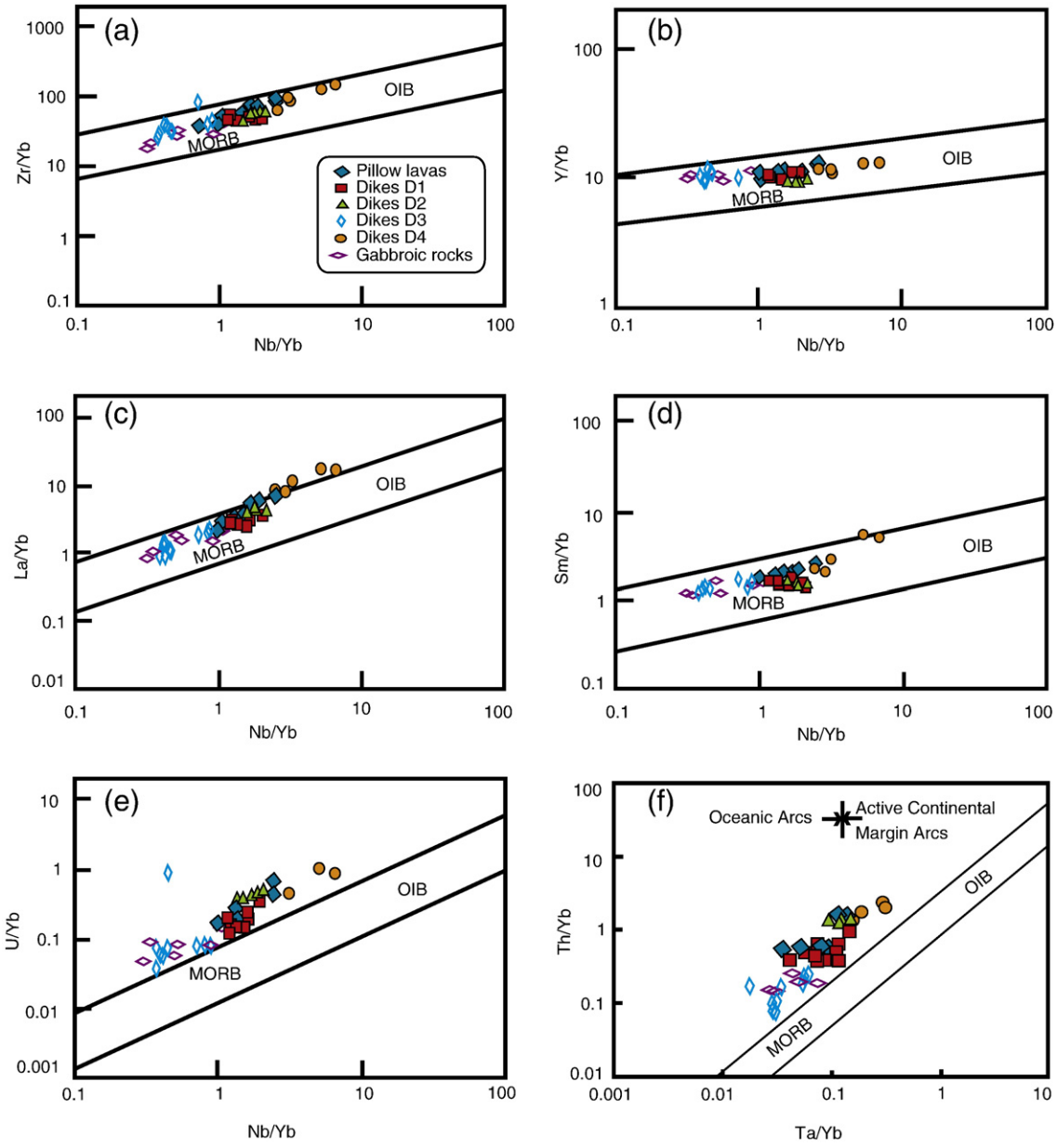

Fig. 9. (a–e) Plot of M/Yb versus Nb/Yb for the ophiolitic rocks and associated dikes in the Wadi Ghadir area where M is (a) Zr, (b) Y, (c) La, (d) Sm, (e) U. MORB and OIB represent the position of the mid-ocean ridge and oceanic island mantle source respectively. Mantle array (MORB-OIB array) after Green (2006). (f) Th/Yb versus Ta/Yb diagrams with mantle array after Pearce (1983).

from the subducted slab; it is also influenced by subduction-induced corner flow (Ewart and Hawkesworth 1987). This counter flow mantle convection provides a continuous supply of fertile mantle, but due to back-arc extension and melt extraction, the mantle advected into the wedge beneath the arc undergoes depletion (McCulloch and Gamble, 1991; Hawkins, 2003). The nature of back-arc magmatism is a result of mixing of a MORB-like source and limited enrichment in LILE relative to arc magmatism (Taylor and Martinez, 2003). The degree of mixing of these components is controlled by the distance to the island arc (Sinton et al., 2003). The inferred back-arc basin origin of the WGO is consistent with previous studies (El Bayoumi and Greiling, 1984; Kröner, 1985; Kröner et al., 1987; Farahat et al., 2004).

Because all analyzed samples have TiO_2 contents more than 1 wt.%, the WGO can be classified, following Serri (1981), as a high-Ti ophiolite. In this sense, the WGO compares well with some other Tethyan ophiolites such as, Troodos in Cyprus and Semail in Oman and the Proterozoic ophiolites in the ANS such as Jabal Al Wask in Saudia

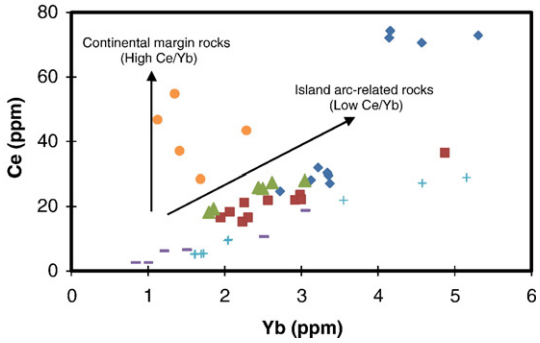

Fig. 10. Variation of Ce and Yb contents in the ophiolitic rocks of Wadi Ghadir and associated dikes. Island arc (low Ce/Yb) and continental margin (high Ce/Yb) trends after Hawkesworth et al. (1993). Symbols as in Fig. 5.

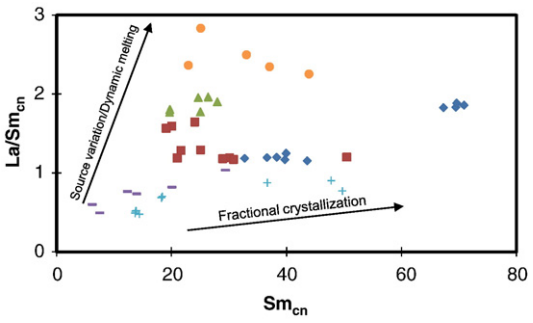

Fig. 11. Variation of La/Sm$_{cn}$ and Sm in the ophiolitic and associated rocks of the Wadi Ghadir area. Source variation and/or dynamic melting trend and fractional crystallization trend after Pearce et al. (1995). Symbols as in Fig. 5.

Arabia and Onib in Sudan (Zimmer et al., 1995; Hussein et al., 2004 and references therein). Using the criteria in Pearce et al. (1984) and Pearce (2008), we infer that the chemical signature, the crystallization sequence, mantle residue and Y proxy of the WGO are similar to most supra-subduction zone ophiolites formed in back-arc basins. On the Ti–V variation diagram, the WGO samples overlap with recent back-arc basins fields such as the Lau and Manus Basins (Fig. 13a). The WGO have higher La/Sm$_{cn}$ values than the Lau Basin samples, but are within the range of the Manus Basin samples and their Nb/La$_{pm}$ ratios is similar to that of both the Lau and Manus Basins (Fig. 14a, b, c). The Lau Basin has higher Nb/Th$_{pm}$ ratio than the WGO, but the latter still has a Nb/Th$_{pm}$ ratio within the range of the Manus Basin, confirming its back-arc tectonic setting (Fig. 14d). Regarding its La/Sm$_{cn}$ ratio, the WGO overlaps with the Betts Cove (Bédard, 1999), Oman (Godard et al., 2006) and the Dagzhuka–Tibet (Xia et al., 2003) ophiolites. It also overlaps with the Oman ophiolites in terms of its TiO_2 and Zr contents and Nb/Th$_{pm}$ ratios and with the Betts Cove and Tibet fore-arc ophiolites, in terms of its Nb/Th$_{pm}$ ratios (Fig. 14). The high TiO_2 and Zr values of the WGO were also reported by El Bayoumi (1980). His TiO_2 and Zr values range from 0.74 to 3.64 wt.% and from 27 to 448 ppm, respectively.

The Wadi Ghadir area is a part of a mélange separated from the Hafafit gneissic dome by the volcanic and volcaniclastic rocks of the Nugrus volcanic arc complex (Abd El-Naby and Frisch, 2006). We infer that the Nugrus arc developed as a SW-facing intra-oceanic arc system above a NE-dipping (in present coordinate system) subduction zone, and that the WGO was situated in a back-arc setting behind that Nugrus volcanic arc, tapping into a fertile MORB mantle source (Fig. 15a).

The late-stage D4 dikes have unique characteristics relative to the other rocks in the study area. These dikes are calc-alkaline in composition, and although their MORB-normalized patterns are similar to the other subduction-related rocks (i.e. enriched in LILE relative to HFSE and negative Nb and Ta anomalies), they have stronger enrichment in LILE than the WGO and its associated dikes.

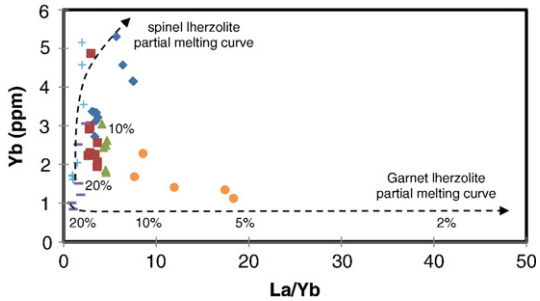

Fig. 12. Variation of La/Yb versus Yb for ophiolitic rocks and associated dikes of the Wadi Ghadir area. Modal melting curves of garnet–lherzolite and spinel–lherzolite sources derived from Baker et al. (1997) but scale for percentage of melting of mantle after Rotolo et al. (2006). Symbols as in Fig. 5.

They also differ from the other rocks by higher concentrations of Nb and Ta relative to Zr and of Zr relative to Y and Yb (Table 3). These features indicate contributions from a mantle source enriched in incompatible elements, such as sub-continental lithospheric mantle (Pearce, 1983). These geochemical characteristics and also the similarity between chondrite-normalized REE patterns of D4 dikes and the calc-alkaline volcanic rocks of an Andean magmatic arc (Thorpe et al., 1984; D'Orazio et al., 2003) suggest their generation in an active continental margin setting.

D4 dikes may mark the onset of calc-alkaline volcanism in the area characterizing the transformation of the passive continental margin into an active margin after the accretion of Nugrus volcanic arc and its WGO back-arc crust. This is in accordance with Kröner's (1985) model for the evolution of the Nubian part of the ANS. The conversion from a passive continental margin into an active margin was accompanied by a change in subduction polarity following ophiolite emplacement (Fig. 15b). The newly established SW-dipping subduction produced calc-alkaline magmatism in the form of early basaltic dikes (D4 dikes) and leucogabbro intruding the mélange, WGO and Hafafit gneissic dome. The mantle source of D4 dikes included melt-depleted mantle that was previously beneath the Nugrus island arc and enriched sub-continental lithospheric mantle beneath the Hafafit dome. This is shown by the enrichment in highly incompatible elements (e.g. La and Ce) relative to Y and Yb (Fig. 7). With the establishment of a SW-dipping subduction zone, the granitic calc-alkaline plutons and the

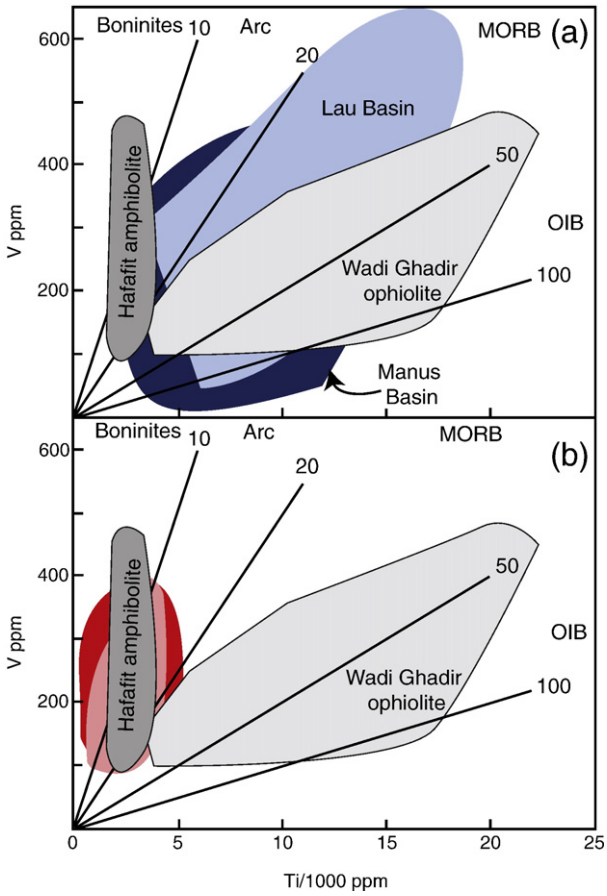

Fig. 13. Ti–V discrimination diagram (Shervais, 1982) for Wadi Ghadir ophiolitic rocks (light gray field) and Hafafit amphibolites (dark gray field) to compare with (a) back-arc basins, Lau Basin (light blue) and Manus Basin (Dark blue); and (b) forearc/arc ophiolites, Betts Cove (Red) and Troodos (Pink). Data for Lau Basin form Pearce et al. (1994); for Manus Basin from Sinton et al. (2003); for Betts Cove ophiolite from Bédard (1999); and for Troodos ophiolite from Flower and Levine (1987).

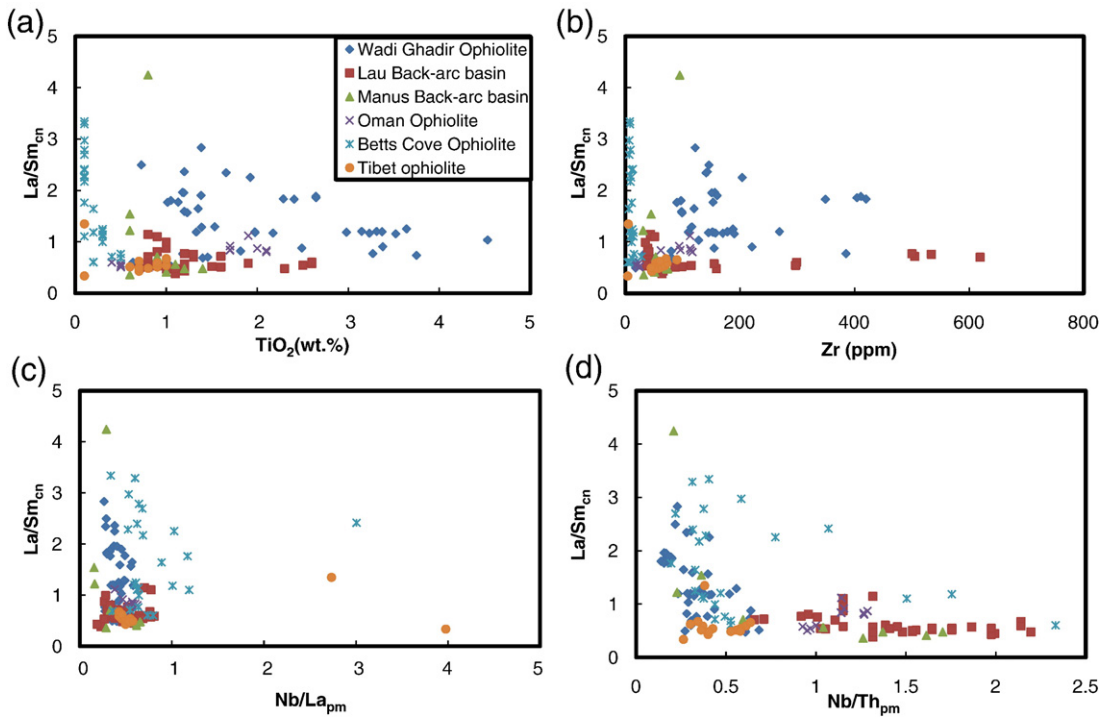

Fig. 14. Comparison of the Wadi Ghadir ophiolitic rocks with back-arc basins and different ophiolites through (a) TiO_2 versus La/Sm_{cn}; (b) Zr versus La/Sm_{cn}; (c) Nb/La_{pm} versus La/Sm_{cn}; and (d) Nb/Th_{pm} versus La/Sm_{cn}. Data for Lau Basin form Pearce et al. (1994); for Manus Basin from Sinton et al. (2003); for Betts Cove ophiolite from Bédard (1999); for Dagzhuka (Tibet) from Xia et al. (2003); and for Oman ophiolite from Godard et al. (2006).

leucogabbro of the new Andean-type continental margin formed (El Bayoumi, 1980, 1983; Takla et al., 1992). These plutonic rocks include mafic xenoliths derived from the WGO and the ophiolitic mélange.

7. Conclusions

The geochemical characteristics of the gabbros and pillow lavas of the WGO are consistent with their origin in a back-arc basin tectonic

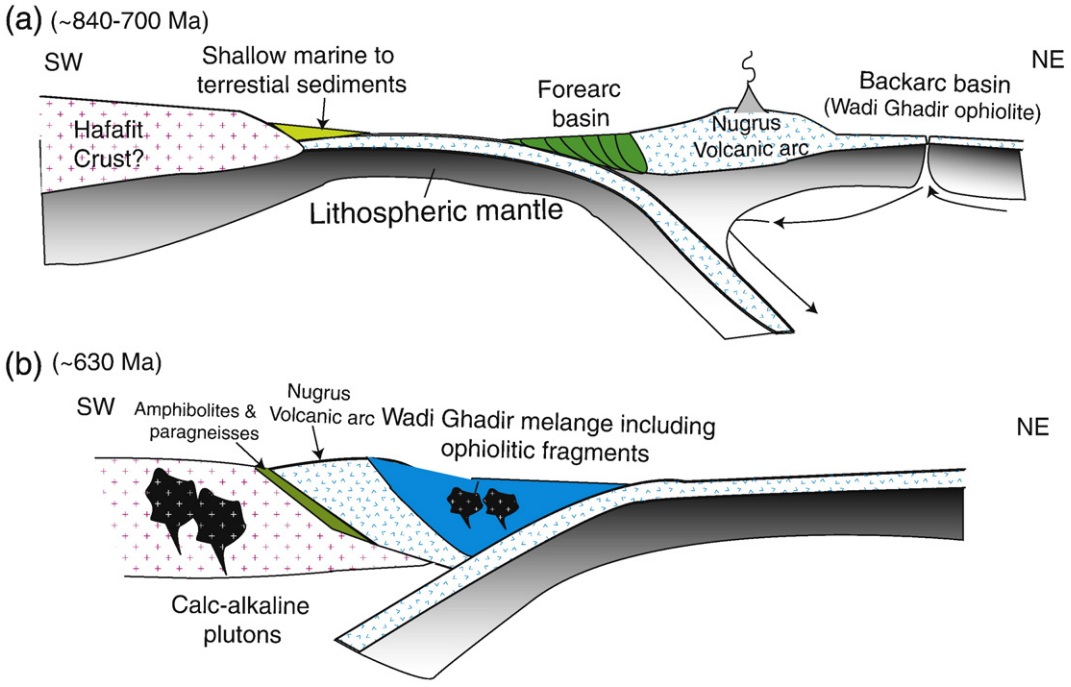

Fig. 15. Tectonic model for evolution of the Wadi Ghadir area relative to the Nugrus unit and Hafafit from oceanic crust to active continental margin. (a) Partial melting of mantle beneath back-arc during formation of the Wadi Ghadir ophiolitic rocks. Arrows show approximate direction of flow and how the mantle beneath Nugrus arc becomes isolated relative to fertile mantle and recipient only to depleted flow from back-arc rift/spreading area. (b) Collision of Nugrus arc system with Hafafit block (old mature arc or crust) resulted in a reversal of subduction polarity from east to west. The reversal of subduction polarity led to formation of accretion area behind the collision zone and the beginning of calc-alkaline magmatism (D4 dikes and probably leucogabbro) and to transformation of the Wadi Ghadir area from oceanic crust to active continental margin. At the collision zone the sediments of Hafafit and forearc of Nugrus arc are squeezed and transformed into amphibolite, mylonite and paragneisses. Northeast and southwest directions are present-day directions. Locations are in present coordinate system, ages are approximate after Stern (2007).

setting. The ophiolitic rocks and D1, D3 dikes intruding them were derived from melting of slightly depleted to fertile N-MORB mantle. The garnet signature can be attributed to melting of a spinel peridotite mantle, veined or layered, with garnet pyroxenite. On the other hand, the geochemistry of calc-alkaline D4 dikes and granitoid plutons intruding the WGO and the ophiolitic mélange represent active continental margin products that formed after ophiolite emplacement via an arc-passive margin collision. Magmas of D4 dikes likely originated from melting of fertile N-MORB mantle that had been affected by contributions from sub-continental lithosphere mantle and/or garnet–peridotite mantle. The porphyritic pillow lavas and D2 dikes have intermediate geochemical characteristics between the two groups, and we attribute their origin to a transitional tectonic setting between the back-arc setting and the onset of active continental margin magmatism, following a subduction polarity change after the emplacement of the WGO and the Nugrus volcanic arc onto Hafafit passive margin.

Acknowledgements

We thank J.C. Barrette, J.C. Ordóñez-Calderón and Zhaoping Yang for their help during geochemical analyses. Reviewers A. Kröner and J. Dostal are acknowledged for their comprehensive and incisive critiques on the manuscript, which have resulted in significant improvements to the paper. We thank N. Eby for his constructive editorial comments. PREA and NSERC grants (250926) of A. Polat and NSERC grant (83117) of B. Fryer are greatly acknowledged.

References

Abd El-Naby, H., Frisch, W., 2006. Geochemical constraints from the Hafafit Metamorphic Complex (HMC): evidence of Neoproterozoic back-arc basin development in the central Eastern Desert of Egypt. Journal of African Earth Sciences 45, 173–186.

Abdelsalam, M.G., Stern, R.J., 1996. Sutures and shear zones in the Arabian–Nubian Shield. Journal of African Earth Sciences 23, 289–310.

Ahmed, A.H., Arai, S., Attaia, A.K., 2001. Petrological characteristics of the Pan African podiform chromatite and associated peridotites of the Proterozoic ophiolite complexes, Egypt. Mineralium Deposita 36, 72–84.

Azer, M.K., Stern, R.J., 2007. Neoproterozoic (835–720) serpentinites in the Eastern Desert, Egypt: fragments of forearc mantle. The Journal of Geology 115, 457–472.

Baker, J.A., Menzies, M.A., Thirlwall, M.F., Macpherson, C.G., 1997. Petrogenesis of Quaternary intraplate volcanism, Sana'a, Yemen: implications for plume–lithosphere interaction and polybaric melt hybridization. Journal of Petrology 38, 1359–1390.

Barrett, T.J., MacLean, W.H., 1994. Chemostratigraphy and hydrothermal alteration in exploration for VHMS deposits in greenstone and younger volcanic rocks. In: Lentz, D.R. (Ed.), Alteration and Alteration Processes Associated with Ore-Forming Systems. Geological Association of Canada, Short Course Notes, vol. 11, pp. 433–467.

Bédard, J.H., 1999. Petrogenesis of boninites from the Betts Cove ophiolite, Newfoundland, Canada: identification of subducted source component. Journal of Petrology 40, 1853–1889.

Church, W.R., 1988. Ophiolites, sutures, and micro-plates of the Arabian–Nubian Shield: a critical comment. In: El-Gaby, S., Greiling, R.O. (Eds.), The Pan-African Belt of Northeast Africa and Adjacent Areas: Tectonic Evolution and Economic Aspects of a Late Proterozoic Orogen, Friedrich. Vieweg, Sohn Verlagsgesellschaft mbH, pp. 289–316.

Class, C.D., Miller, D.M., Goldstein, S.L., Langmuir, C.H., 2000. Distinguishing melt and fluid subduction components in Umnak volcanics, Aleutian arc. Geochemistry, Geophysics, and Geosystems 1 paper number 1999GC000010.

D'Orazio, M., Innocenti, F., Manetti, P., Tamponi, M., Tonarini, S., González-Ferrán, O., Lahsen, A., Omarini, R., 2003. The Quaternary calc-alkaline volcanism of the Patagonian Andes close to the triple junction: geochemistry and petrogenesis of volcanic rocks from the Cay and Maca volcanoes (≈45°S, Chile). Journal of South America Earth Sciences 16, 219–242.

Dilek, Y., 2003. Ophiolite pulses, mantle plumes and orogeny. In: Dilek, Y., Robinson, P.T. (Eds.), Ophiolite in Earth History. Geological Society, London, Special Publication, vol. 218, pp. 9–19.

Dilek, Y., Ahmed, Z., 2003. Proterozoic ophiolites of the Arabian Shield and their significance in Precambrian tectonics. In: Dilek, Y., Robinson, P.T. (Eds.), Ophiolite in Earth History. Geological Society, London, Special Publication, vol. 218, pp. 685–700.

Dostal, J., Strong, D.F., Jamieson, R.A., 1980. Trace element mobility in the mylonite zone within the ophiolite aureole, St. Anthony Complex, Newfoundland. Earth and Planetary Science Letters 49, 188–192.

El Bayoumi, R.M., 1980. Ophiolites and associated rocks of Wadi Ghadir, east of Gabal Zabara, Eastern Desert, Egypt. Ph.D. Thesis, Cairo University, Egypt, 171 pp.

El Bayoumi, R.M., 1983. Ophiolites and mélange complex of Wadi Ghadir area, Eastern Desert, Egypt. Bulletin of King Abdelaziz University 6, 329–342.

El Bayoumi, R.M.A., Greiling, R.O., 1984. Tectonic evolution of a Pan-African plate margin in southeastern Egypt — a suture zone overprinted by low angle thrusting? In: Klerkx, J., Michot, J. (Eds.), Géologie Africaine-African Geology. Musee royal de l'Africaine Centrale, Tervuren, Belg, pp. 47–56.

El Gaby, S., List, F.K., Tehrani, R., 1988. Geology, evolution and metallogenesis of the Pan-African belt in Egypt. In: El Gaby, S., Greiling, R.O. (Eds.), The Pan-African Belt of Northeast Africa and Adjacent Areas: Tectonic Evolution and Economic Aspects of a Late Proterozoic Orogen, Friedrich. Vieweg, Sohn Verlagsgesellschaft mbH, pp. 17–68.

El Sayed, M.M., Furnes, H., Mohamed, F.H., 1999. Geochemical constraints on the tectonomagmatic evolution of the late Precambrian Fawakhir ophiolite, central Eastern Desert, Egypt. Journal of African Earth Sciences 29, 515–533.

El Sharkawy, M.A., El Bayoumi, R.M., 1979. The ophiolites of Wadi Ghadir area Eastern Desert, Egypt. Annals of the Geological Survey of Egypt IX, 125–135.

Ewart, A., Hawkesworth, C.J., 1987. The Pleistocene–Recent Tonga–Kermadec arc lavas: interpretation to new isotopic and rare earth data in terms of a depleted mantle source model. Journal of Petrology 28, 495–530.

Farahat, E.S., El Mahalawi, M.M., Hoinkes, G., Abdel Aal, A.Y., 2004. Continental back-arc basin origin of some ophiolites from the Eastern Desert of Egypt. Mineralogy and Petrology 82, 81–104.

Flower, M.F.J., Levine, H.M., 1987. Petrogenesis of a tholeiite–boninite sequence from Ayios Mamas, Troodos ophiolite: evidence for splitting of a volcanic arc? Contribution to Mineralogy and Petrology 97, 509–524.

Gillis, K.M., Banerjee, N.R., 2000. Hydrothermal alteration patterns in supra-subduction zone ophiolites. In: Dilek, Y., Moores, E.M., Elthon, D., Nicolas, A. (Eds.), Ophiolites and Oceanic Crust: New Insights from Field Studies and the Ocean Drilling Program. Boulder, Colorado, Geological Society of America Special Paper, vol. 349, pp. 283–297.

Godard, M., Bosch, D., Einaudi, F., 2006. A MORB source for low-Ti magmatism in the Semail ophiolite. Chemical Geology 234, 58–78.

Green, N.L., 2006. Influence of slab thermal structure on basalt source regions and melting conditions: REE and HFSE constraints from the Garibaldi volcanic belt, northern Cascadia subduction system. Lithos 87, 23–49.

Hassanien, S.M., 2001. Volcano-sedimentary sequence of Gabal Um Khariga, Central Eastern Desert, Egypt. Egyptian Journal of Geology 45, 65–88.

Hawkesworth, C.J., Gallagher, K., Hergt, J.M., McDermott, F., 1993. Mantle and slab contributions in arc magmas. Annual Review of Earth and Planetary Sciences 21, 175–204.

Hawkesworth, C.J., Turner, S.P., McDermott, F., Peate, D.W., van Calsteren, P., 1997. U–Th isotopes in arc magmas: implications for element transfer from the subducted crust. Science 276, 551–555.

Hawkins, J.W., 2003. Geology of supra-subduction zones—implications for the origin of ophiolites. In: Dilek, Y., Newcomb, S. (Eds.), Ophiolite Concept and the Evolution of Geological Thought. Boulder, Colorado, Geological Society of America Special Paper, vol. 373, pp. 227–268.

Hirschmann, M.M., Stolper, E.M., 1996. A possible role for garnet pyroxenite in the origin of the "garnet signature" in MORB. Contribution to Mineralogy and Petrology 124, 185–208.

Humphries, S.E., 1984. The mobility of the rare earth elements in the crust. In: Henderson, P. (Ed.), Rare Earth Element Geochemistry. Elsevier, Amsterdam, pp. 317–342.

Hussein, I.M., Kröner, A., Reischmann, T., 2004. The Wadi Onib mafic–ultramafic complex: a Neoproterozoic supra-subduction zone ophiolite in the northern Red Sea Hills of the Sudan. In: Kusky, T.M. (Ed.), Precambrian Ophiolites and Related Rocks. Developments in Precambrian Geology, vol. 13. Elsevier, Amsterdam, pp. 163–206.

Jenner, G.A., Longerich, H.P., Jackson, S.E., Fryer, B.J., 1990. ICP-MS — a powerful tool for high-precision trace-element analysis in earth sciences: evidence from analysis of selected U.S.G.S. reference samples. Chemical Geology 83, 133–148.

Kessel, R., Schmidt, M.W., Ulmer, P., Pettke, T., 2005. Trace element signature of subduction-zone fluids, melts and supercritical fluids at 120–180 km depths. Nature 437, 724–727.

Khalil, K.I., 2007. Chromite mineralization in ultramafic rocks of the Wadi Ghadir area, Eastern Desert, Egypt: mineralogical, microchemical and genetic study. Neues Jahrbuch für Mineralogie — Abhandlungen 183, 283–296.

Kröner, A., 1985. Ophiolites and the evolution of tectonic boundaries in the late Proterozoic Arabian–Nubian Shield of northeast Africa and Arabia. Precambrian Research 27, 277–300.

Kröner, A., Greiling, R.O., Reischmann, T., Hussein, I.M., Stern, R.J., Durr, S., Kruger, J., Zimmer, M., 1987. Pan-African crustal evolution in the Nubian segment of northeast Africa. In: Kröner, A. (Ed.), Proterozoic Lithospheric Evolution. American Geophysical Union. Geodynamics Series, vol. 17, pp. 237–257.

Kröner, A., Todt, W., Hussein, I.M., Mansour, M., Rashwan, A.A., 1992. Dating of late Proterozoic ophiolites in Egypt and the Sudan using the single grain zircon evaporation technique. Precambrian Research 59, 15–32.

Kröner, A., Windley, B.F., Badarch, G., Tomurtogoo, O., Hegner, E., Jahn, B.M., Gruschka, S., Khain, E.V., Demoux, A., Wingate, M.T.D., 2007. Accretionary growth and crustal formation in the Central Asian Orogenic Belt and comparison with the Arabian–Nubian Shield. In: Hatcher, R.D., CarlsonJr. Jr., M.B., MacBride, J.H., Catalan, J.M. (Eds.), 4-D Framework of the Continental Crust—In Targeting Crustal Processes Through Time. Geological Society of America, Memoir, vol. 200, pp. 181–209.

Martinez, F., Taylor, B., 2003. Controls on back-arc crustal accretion: insights from the Lau, Manus and Mariana basins. In: Larter, R.D., Leat, E.T. (Eds.), Intra-oceanic Subduction Systems: Tectonic and Magmatic Processes. Geological Society, London, Special Publication, vol. 219, pp. 19–54.

McCulloch, M.T., Gamble, J.A., 1991. Geochemical and geodynamical constraints on subduction zone magmatism. Earth Planet Science Letters 102, 358–374.

Pearce, J.A., 1982. Trace element characteristics of lavas from destructive plate boundaries. In: R.S., Thorpe (Ed.), Andesites: Orogenic Andesites and Related Rocks. John Wiley, Chichester, pp. 525–547.

Pearce, J.A., 1983. Role of sub-continental lithosphere in magma genesis at active continental margins. In: Hawkesworth, C.J., Norry, M.J. (Eds.), Continental Basalts and Mantle Xenoliths. Shiva, Nantwich, UK, pp. 230–249.
Pearce, J.A., 2003. Supra-subduction zone ophiolites: the search for modern analogues. In: Dilek, Y., Newcomb, S. (Eds.), Ophiolite Concept and the Evolution of Geological Thought. Boulder, Colorado, Geological Society of America Special Paper, vol. 373, pp. 269–295.
Pearce, J.A., 2008. Geochemical fingerprinting of oceanic basalts with applications to ophiolite classification and the search for Archean oceanic crust. Lithos 100, 14–48.
Pearce, J.A., Baker, P.E., Harvey, P.K., Luff, I.W., 1995. Geochemical evidence for subduction fluxes, mantle melting and fractional crystallization beneath the South Sandwich island arc. Journal of Petrology 36, 1073–1109.
Pearce, J.A., Ernewein, M., Bloomer, S.H., Parson, L.M., Murton, B.J., Johnson, L., 1994. Geochemistry of Lau Basin volcanic rocks: influence of ridge segmentation and arc proximity. In: Smellie, J.L. (Ed.), Volcanism Associated with Extension at Consuming Plate Margins. Geological Society, London, Special Publication, vol. 81, pp. 53–75.
Pearce, J.A., Lippard, S.J., Roberts, S., 1984. Characteristics and tectonic significance of supra-subduction zone ophiolites. In: Kokelaar, P.B., Howells, M.F. (Eds.), Marginal Basin Geology. Geological Society, London, Special Publication, vol. 16, pp. 77–94.
Pearce, J.A., Peate, D.W., 1995. Tectonic implications of the composition of volcanic arc lavas. Annual Review of Earth and Planetary Sciences 23, 251–285.
Polat, A., Hofmann, A.W., 2003. Alteration and geochemical patterns in the 3.7–3.8 Ga Isua greenstone belt, West Greenland. Precambrian Research 126, 197–218.
Polat, A., Hofmann, A.W., Rosing, M.T., 2002. Boninite-like volcanic rocks in the 3.7–3.8 Ga Isua greenstone belt, West Greenland: geochemical evidence for intra-oceanic subduction zone processes in the early Earth. Chemical Geology 184, 231–254.
Ragland, P.C., 1989. Basic Analytical Petrology. Oxford University Press, New York.
Ramly, M.F., Soliman, F.A., Rasmy, A.H., Abu El Farh, M.H., 1998. Petrographic and geochemical characteristics of the island arc rocks in the area between Wadi Garf and Wadi Um Khariga, Central Eastern Desert of Egypt. Annals of the Geological Survey of Egypt 1–22 V.XXI.
Reischmann, T., 2000. Ophiolites and island arcs in the late Proterozoic Nubian Shield. Ofioliti 25, 1–13.
Ries, A.C., Shackleton, R.M., Graham, R.H., Fitches, W.R., 1983. Pan-African structures, ophiolites and mélanges in the Eastern Desert of Egypt: a traverse at 26° N. Journal of Geological Society, London 140, 75–95.
Rollinson, H.R., 1993. Using Geochemical Data: Evaluation, Presentation and Interpretation. Longman/Wyllie. Harlow/New York.
Rotolo, S.G., Castorina, F., Cellura, D., Pompilio, M., 2006. Petrology and geochemistry of submarine volcanism in the Sicily channel rift. The Journal of Geology 114, 355–365.
Şengör, A.M.C., Natal'in, B.A., 1996. Turkic-type orogeny and its role in the making of the continental crust. Annual Review of Earth Planet Science 24, 263–337.
Şengör, A.M.C., Natal'in, B.A., 2004. Phanerozoic analogues of Archaean oceanic basement fragments: Altaid ophiolites and orogens. In: Kusky, T.M. (Ed.), Precambrian Ophiolites and Related Rocks. Developments in Precambrian Geology. Elsevier, Amsterdam, vol. 13, pp. 675–726.
Serri, G., 1981. The petrochemistry of ophiolite gabbroic complexes: a key for the classification of ophiolites into low-Ti and high-Ti types. Earth and Planetary Science Letters 52, 203–212.
Shackleton, R.M., Ries, A.C., Graham, R.H., Fitches, W.R., 1980. Late Precambrian ophiolite mélange in the eastern desert of Egypt. Nature 285, 472–474.
Shervais, J.W., 1982. Ti–V plots and the petrogenesis of modern and ophiolitic lavas. Earth Planetary Science Letters 59, 101–118.
Sinton, J.M., Ford, L.L., Chappell, B., McCulloch, M.T., 2003. Magma genesis and mantle heterogeneity in the Manus back-arc basin, Papua New Guinea. Journal of Petrology 44, 159–195.
Stern, R.J., 1994. Arc assembly and continental collision in the Neoproterozoic East African Orogen: implications for the consolidation of Gondwanaland. Annual Review of Earth and Planet Sciences 22, 319–351.
Stern, R.J., 2004. Subduction initiation: spontaneous and induced. Earth Planetary Science Letters 266, 275–292.
Stern, R.J., 2005. Evidence from ophiolites, blueschists, and ultrahigh-pressure metamorphic terranes that modern episodes of subduction tectonics began in Neoproterozoic time. Geology 33, 557–560.
Stern, R.J., 2007. Neoproterozoic crustal growth: the solid Earth system during a critical episode of Earth history. Gondwana Research 14, 33–50.
Stern, R.J., Johanson, P.R., Kröner, A., Yibas, B., 2004. Neoproterozoic ophiolites of the Arabian–Nubian Shield. In: Kusky, T.M. (Ed.), Precambrian Ophiolites and Related Rocks. Developments in Precambrian Geology, vol. 13. Elsevier, Amsterdam, pp. 95–128.
Sultan, M., Bickford, M.E., El Kaliouby, B., Arvidson, R.E., 1992. Common Pb systematics of Precambrian granitic rocks of the Nubian shield (Egypt) and tectonic implications. Geological Society of American Bulletin 104, 456–470.
Sun, S.-S., McDonough, W.F., 1989. Chemical and systematic of oceanic basalts: implications for mantle composition and processes. In: Saunders, A.D., Norry, M.J. (Eds.), Magmatism in Ocean Basins. Geological Society, London, Special Publication, vol. 42, pp. 313–345.
Takla, M.A., Basta, F.F., Shenouda, H.H., El-Maghraby, A.M., 1992. Geochemistry of gneisses and granitoids of Wadi Ghadir area, Eastern Desert, Egypt. Geology of the Arab World 1st., pp. 477–506.
Takla, M.A., Hassanien, S., Sakran, S., 1990. Geochemistry of the ophiolitic mélange between Idfu-Marsa Alam Road and Wadi Shait, Eastern Desert, Egypt. Egyptian Mineralogist 2, 31–50.
Tatsumi, Y., Kogiso, T., 2003. The subduction factory: its role in the evolution of the Earth's crust and mantle. In: Larter, R.D., Leat, E.T. (Eds.), Intra-oceanic Subduction Systems: Tectonic and Magmatic Processes. Geological Society, London, Special Publication, vol. 219, pp. 55–80.
Taylor, B., Martinez, F., 2003. Back-arc basin basalt systematic. Earth and Planetary Science Letters 210, 481–497.
Thorpe, R.S., Francis, P.W., O'Callaghan, L., 1984. Relative roles of source composition, fractional crystallization and crustal contamination in the petrogenesis of Andean volcanic rocks. Philosophical Transactions of the Royal Society of London (A) 310, 675–692.
Winchester, J.A., Floyd, P.A., 1976. Geochemical magma type discrimination: application to altered and metamorphosed basic igneous rocks. Earth and Planetary Science Letters 28, 459–469.
Winchester, J.A., Floyd, P.A., 1977. Geochemical discrimination of different magma series and their differentiation products using immobile elements. Chemical Geology 20, 325–343.
Woodhead, J., Eggins, S., Gamble, J., 1993. High-field-strength and transition element systematics in island-arc and back-arc basin basalts—evidence for multiphase melt ex-traction and a depleted mantle wedge. Earth and Planet Science Letters 114, 491–504.
Woodhead, J.D., Hergt, J.M., Davidson, J.P., Eggins, S.M., 2001. Hafnium isotope evidence for 'conservative' element mobility during subduction processes. Earth and Planetary Science Letters 192, 331–346.
Xia, B., Yu, H., Chen, G., Qi, L., Zhao, T., Zhou, M., 2003. Geochemistry and tectonic environment of the Dagzhuk ophiolite in the Yarlung-Zangbo suture zone, Tibet. Geochemical Journal 37, 311–324.
Zimmer, M., Kröner, A., Jochum, K.P., Reischmann, T., Todt, W., 1995. The Gabal Gerf complex: a Precambrian N-MORB ophiolite in the Nubian Shield, NE Africa. Chemical Geology 123, 29–51.